

Article

# Variable Admittance Control in Sliding Mode for Robust Physical Human–Robot Interaction

Jingdong Chen and Paul I. Ro \*

Department of Mechanical Engineering, School of Engineering & Computer Science, Baylor University, Waco, TX 76798, USA; jingdong\_chen@baylor.edu

\* Correspondence: paul\_ro@baylor.edu

**Abstract:** Intuitive and comfortable physical human–robot interaction (pHRI) can be realized by changing impedance/admittance parameters corresponding to human interaction. However, this dynamic adjustment may result in drastically changed system dynamics, which usually give rise to system instability. We introduce a power envelope regulation strategy designed to constrain the variability of admittance parameters, thereby ensuring system passivity and mitigating the risk of instability. Then, sliding mode control (SMC) is employed to yield stable and robust performance. A new sliding surface is proposed based on feedback linearization, which shows improved tracking performance and stability compared to a conventional sliding surface. The effectiveness of the proposed sliding surface and associated control is theoretically validated. Notably, our modified sliding surface works universally, regardless of the order of the desired admittance equation. The trade-off between system chattering and robustness is effectively managed using a variable–boundary approach, which dynamically adjusts system constraints to optimize performance. In addition, a control algorithm combining acceleration feedback and sliding mode is proposed, showing improved robustness and tracking accuracy performance compared with applying the proposed SMC algorithm exclusively. The efficacy of these methodologies is substantiated through numerical simulations and empirical experiments.

**Keywords:** physical human–robot interaction; human intention adaptation; variable admittance control (VAC); passivity and stability; power envelope; sliding mode control (SMC); acceleration feedback



**Citation:** Chen, J.; Ro, P.I. Variable Admittance Control in Sliding Mode for Robust Physical Human–Robot Interaction. *Appl. Sci.* **2023**, *13*, 11219. <https://doi.org/10.3390/app132011219>

Academic Editor: Alessandro Di Nuovo

Received: 29 August 2023  
Revised: 29 September 2023  
Accepted: 9 October 2023  
Published: 12 October 2023



**Copyright:** © 2023 by the authors. Licensee MDPI, Basel, Switzerland. This article is an open access article distributed under the terms and conditions of the Creative Commons Attribution (CC BY) license (<https://creativecommons.org/licenses/by/4.0/>).

## 1. Introduction

By leveraging robots' strengths in precision, speed, and efficiency with humans' cognitive abilities and dexterity, physical human–robot cooperation leads to better performance in tasks requiring high flexibility and complexity [1–6]. Effective physical human–robot interaction (pHRI) relies on the knowledge of variable human dynamics and intention [7–10]. In certain applications like mobility aids for individuals with motor decline or impairments, the robot takes on a dominant role that demands a higher level of intelligence [11–13]. In this regard, sufficient knowledge about humans, e.g., human intention, is crucial to the robot [14–16]. Another crucial aspect of this interactive control is the realization of compliance and stiff motion depending on the specific tasks being executed [16]. Interaction force is one of the most straightforward signals used to convey human intention with physical interaction involved [15–18]. As per the human interaction force, the interactive controllers were studied to realize the desired dynamic response of the robot. This paper considers the well-known admittance control, as discussed in [17,19–21].

Admittance control takes the force as input and regulates the desired motion via admittance parameters. In physical human–robot interaction (pHRI), input force is highly random, corresponding to various human intentions. The admittance parameters must be updated in real-time to achieve the desired interaction. Variable damping dominantly determines the human's perception of motion in pHRI. The work conducted by Duchaine

and Gosselin selected the time derivative of interaction force to infer the human's future intention (i.e., acceleration and deceleration) where the damping decreases according to a suddenly increased force and vice versa [22]. A similar force-dependent approach was proposed in [18], where the direction of force and velocity was introduced to detect acceleration and deceleration. A common disadvantage of these methods is that the user must continuously exert higher force to maintain a long-duration, faster motion. Chen and Ro [16] addressed this issue by proposing an updating rule for damping that saves the user's efforts. Virtual stiffness is usually omitted because restoring the forces in a virtual spring is not desirable when the human leads the robot to move in free space. Inducing a stiffness force term renders a less compliant behavior of the robot. In contrast, the stiffness term is essential to maintain small position tracking errors upon disturbance if a trajectory is prescribed. In [23,24], active stiffness combined with reference trajectory deduced from human intended motion yields a compliant and effort-saving interaction. Virtual inertia has less direct contributions to human perception of robot motion but critically impacts the system's stability, as discussed in [25,26]. A lower value of inertia is appealing in acceleration and fast movement. Intuitively, small inertia may yield a rapid change in speed to be perceived immediately by the user if the control frequency is high. However, experimental results observed in [16] suggested no significant improvement in human perception experience by increasing inertia.

The selection of admittance parameters not only affects the performance (i.e., adaptation to human intention [10,18,22,27,28]) but also impacts the stability of interaction [29–32]. Human intention adaptation determines the intuitiveness of pHRI but cannot take stability into consideration. Passivity is a sufficient condition for a robot's stability when interacting with a passive environment [31], whereas it is a necessary condition in interaction with humans [16]. The proposed power envelope regulation (PER) approach by Chen and Ro [16] can regulate extremely changed admittance parameters induced by human intention such that the drastic change in the admittance dynamics system is suppressed. Though the power envelope regulation adds a protection layer to system stability, it cannot guarantee system stability analytically. Therefore, a stable controller needs to be applied in addition. The sliding mode controller becomes a natural candidate due to its two merits: (i) dynamic behavior of the system can be tailored by choice of the sliding surface; this flexibility allows the realization of desired admittance and (ii) it is robust against modeling uncertainties and external disturbance [33,34].

SMC is a nonlinear controller that utilizes high-frequency switching feedback control. The first application of SMC in impedance control was the study conducted by Lu and Goldenberg in which the integral of the desired impedance was selected as the sliding surface [35]. A new velocity signal was introduced for tracking, intended to couple impedance and robot dynamics. However, the theoretical analysis was somewhat superficial. Additionally, terms such as reference velocity, actual velocity, command velocity, and this newly introduced velocity were not clearly distinguished, leading to potential confusion. For admittance control in pHRI, SMC has been mainly applied in the rehabilitation exoskeleton [36,37], where the sliding surface was adopted as the conventional one discussed in [33]. The admittance equation is solely solved to obtain the response sent to the robot as commands. Nonetheless, simulation results presented in this study show diminished tracking accuracy using the classical method in admittance control in the absence of a prescribed trajectory (or no stiffness term). In addition, in [35–37], the Coriolis and centrifugal matrix can be uniquely determined due to the system's low degree of freedom (DoF), specifically 2. This unique matrix is then used to derive the reachability of SMC via Lyapunov methods, where the explicit expression of the Coriolis and centrifugal matrix is required. Nonetheless, this approach may not be directly applicable to systems with a higher DoF, where the Coriolis and centrifugal matrix have non-unique solutions. A comparative analysis in Section 3 will better deliver the ideas mentioned above.

Chattering is known as the main limitation of implementing SMC in real applications caused by high-frequency oscillation. Two types of techniques, i.e., quasi-sliding mode

and higher order sliding mode (HOSM), have been proposed to tackle chattering. In quasi-sliding mode, a boundary layer is added to the sliding surface by replacing the signum function with saturation, relay, or hyperbolic tangent function [38,39]. Notwithstanding eliminating chattering, the quasi-sliding mode sacrifices robustness and accuracy. Among many HOSM methods, Super-Twisting second-order sliding mode control (STSMC) gained extensive attention in the literature due to its merit of retaining accuracy and robustness while eliminating chattering [39]. Nonetheless, proof of stability of STSMC in the presence of time-varying admittance parameters is challenging and will not be considered in the paper.

Acceleration feedback control (AFC) has been shown to improve control performance by increasing system bandwidth in previous studies [40–43]. Sedghi et al. conducted a frequency-based analysis for two types of AFC on AT telescope via the Bode plot technique [41]. Analyzing power spectral density shows that acceleration feedback adds another sensitivity transfer function to the servo system, improving performance against perturbation. Aung and Kikuuwe experimentally showed the improved performance of the inner position controller on a 1 DoF manipulator by applying AFC along with the friction compensator [42]. Theoretically, the extended bandwidth contributed by acceleration feedback is due to the phase-lead effect. In addition, the stability of high-gain AFC in robotic control has been theoretically proven in the Lyapunov sense under the perfect rigid body assumption by Studenny and Belanger [44]. In practice, the benefit of AFC is usually deteriorated and may not be applicable due to the existence of high-frequency unstructured dynamics [37,40]. The present paper introduces acceleration feedback in the equivalent control in SMC. The initial results show improved performance in tracking accuracy and robustness.

This work aims to provide a systematic and comparative study on improving tracking performance of SMC in variable admittance control (VAC) to ensure human-intention adaptation and system stability. Application to specific and realistic tasks can be easily extended from this generic study. The main contributions of this work can be summarized as follows:

- Limitations of conventional SMC techniques applied to VAC were thoroughly investigated from perspectives of tracking performance, adaptation to time-varying admittance parameters, reachability condition, and chattering removal.
- A new indirect tracking approach was proposed with a new universal sliding surface, corresponding control law, and theoretical proof, yielding improved VAC tracking performance.
- Reachability condition of the proposed SMC approach for VAC was proved, where the challenge of deriving an analytical solution for Coriolis and centrifugal matrix used in Lyapunov stability proof for a higher DoF system was addressed.
- Acceleration feedback was included in equivalent control, and its capability to improve tracking performance was verified in numerical simulation and experiments.

The rest of this paper is organized as follows. Section 2 presents variable admittance control (VAC) and power envelope regulation (PER). In Section 3, a comparative study is conducted to demonstrate the improvement of using our approach in applying SMC in VAC in four aspects: (i) *selection of sliding surface*; (ii) *reachability*; (iii) *chattering removal*; (iv) *performance*. Numerical simulation results are also included in the discussion to present the ideas better. Section 4 outlines the experimental results, and Section 5 concludes the study.

## 2. Human-Intention-Based VAC and PER

This section first introduces a summarized general human-intention framework. Then, the variable admittance control and power envelope regulation that will be applied along with the SMC in Section 3 are discussed. More details about the control algorithms can be referred to our previous work, i.e., [16].

The present study adopts the speed of motion and interaction force measured by a force/torque (F/T) sensor installed at the endpoint of the manipulator to reflect human intentions. It is important to note that other agents introduced by cooperation tasks will not be included. Only the assistive robot and the human user are of interest. The robot's roles are categorized as (i) a passive follower (corresponding to human-leading); (ii) a compliant leader (corresponding to human-following): active or semi-active. According to the passivity analysis in our previous study (refer to [16]) for a more detailed discussion of human intention and VAC), only variable damping and increased stiffness will be considered here. In the first case, only damping is time-varying, and stiffness is updated proportionally with the applied force in the second case.

### 2.1. Variable Admittance Control

Admittance of a mechanical system refers to a linear relationship between input effort and output flow that is expressed in the Cartesian space as

$$M_d(t)(\ddot{x}_c - \ddot{x}_r) + D_d(t)(\dot{x}_c - \dot{x}_r) + K_d(t)(x_c - x_r) = f_h \quad (1)$$

where  $x_c, x_r \in \mathbb{R}^n$  and their time derivatives represent command and reference trajectories, respectively; reference variables are prescribed and known, while command variables are computed from Equation (1) as the robot's response;  $n \leq 6$  denotes the minimal representation of pose of the end effector under a specific configuration;  $M_d \in \mathbb{R}^{n \times n}$  is desired virtual inertia;  $D_d \in \mathbb{R}^{n \times n}$  is desired virtual damping;  $K_d \in \mathbb{R}^{n \times n}$  is desired virtual stiffness;  $M_d, D_d,$  and  $K_d$  are all symmetric matrices; and  $f_h \in \mathbb{R}^n$  represents interaction force. It is worth mentioning that the actual system states do not appear in targeted admittance since admittance regulates the dynamics of the robot's response to interaction force but has no control over tracking.

The robot has no reference trajectory and acts as a passive follower when the human leads motion in free space. To this end, the virtual stiffness term is omitted in Equation (1). If the inertia is constant, then the system is inherently passive. In this regard, the variable damping is updated considering two aspects: (a) comfortable and effort-saving; (b) safe interaction response (i.e., safe operation speed) of the robot.

In order to save effort for the user, the following updating rule is proposed:

$$D_d(t) = \text{diag}(f_n \cdot \dot{x}(t)) \quad (2)$$

where  $\dot{x}(t)$  represents the actual velocity of the end effector in Cartesian space, dot division denotes that the operation is elementwise,  $f_n \in \mathbb{R}^n$  represents constant nominal interaction force determined by the user's comfort level, and  $\text{diag}(\cdot)$  is an operation used to map each entry of the target vector to be a diagonal element of the diagonal matrix. Velocity in Equation (2) can be regarded as the desired value in a steady state corresponding to nominal force at an instant. In such a way, damping correlating to any desired velocities under nominal force can be obtained or asymptotically obtained. As a result, velocity will be held at a higher value even under the restored nominal force. It enables users to interact with the robot using the lower force they prefer most of the time, such that the limitation of some variable damping models in the [17,22] is relaxed. It is important to note that Equation (2) only applies when the velocity is within a minimum threshold value. Singularity and extremely high damping issues appear when velocity is reduced to or approximately to zero. Human intentions in fine motion (slow motion) are not considered in the scope, and constant damping (correlates to nominal force and velocity determined from task definition) is applied when motion is slow.

Stiffness plays a crucial role when the prescribed trajectory is required, such as sit-to-stand transfer assistance. Its value shall increase to make the robot arm stiff enough if loss of balance or a fall is detected. To this end, a simple updating rule is defined according to the human-applied force:

$$K_d(t) = K_c + \gamma \text{diag}(|f_h(t)|) \quad (3)$$

where  $K_c \in \mathbb{R}^n$  is constant stiffness, and  $\gamma$  is a positive constant used to adjust the tuning rate of stiffness. When interaction is abnormal but supportable, stiffness increases as the human-exerted force increases.

### 2.2. Power Envelope Regulation

Power envelope regulation presented in this section aims to regulate the admittance parameters inferred from human intentions from a perspective of safe interaction and system passivity. The power envelope bounds the injected power to the human–robot coupled system.

Equation (2) allows easier leading by reducing damping when a higher force is applied, representing the human intention of accelerating. Nonetheless, smaller damping renders a less dissipative system. If human-injected power is too high, stability or safety may be compromised. The system’s input power must be regulated by a prescribed power envelope profile to ensure safety. To this end, a soft power envelope is defined as follows:

$$P_{soft}^i = f_n^i \dot{x}_{max}^i \quad i = 1, 2, \dots, n \tag{4}$$

where  $\dot{x}_{max}^i$  denotes the maximum safe speed of operation in each dimension. If the interaction force still yields an increasing velocity greater than the maximum safe velocity, the system should increase the damping. Correspondingly, a new updating rule for variable damping will be adopted when the injected power exceeds the soft power envelope, which is given as

$$D_d(t) = \text{diag}\left(\dot{f}_h(t) \cdot \tilde{\dot{x}}_{max}\right) \tag{5}$$

Stability is an overarching safety condition in pHRI and takes precedence over tracking performance. Therefore, constraints on stiffness should also be imposed by including the passivity condition. Though satisfying the passivity condition does not guarantee stability, it suppresses stiffness from increasing excessively. Ferraguti et al. suggested that increasing stiffness injects extra power into the system [31]. Therefore, to maintain the passivity as an additional safety measure against instability, the following constraint is added to the variable stiffness:

$$\frac{1}{2} \dot{K}_d^i(t) \tilde{x}_i^2 \leq \mu D_d^i \tilde{\dot{x}}_i^2, \quad i = 1, 2, \dots, n \tag{6}$$

where  $0 < \mu < 1$ . The power envelope for regulating an extra injected power due to a time-varying stiffness is set on dissipative power, i.e.,  $D_d^i \tilde{\dot{x}}_i^2$ .

## 3. Reachability in VAC

This section presents a fundamental comparative study on SMC in realizing desired admittance. Firstly, the classical and the proposed sliding surfaces are compared in two cases: (i) trajectory tracking (i.e., no interaction); (ii) admittance control. Then, the sliding mode gain is derived according to the Lyapunov stability condition considering time-varying admittance parameters. Section 3.4 introduces the variable boundary layer technique for chattering removal. In the end, the acceleration feedback is included in equivalent control to improve performance further. Numerical simulation is conducted in SIMULINK (MathWorks, Inc., Natick, MA, USA). Certain assumptions have been made for a comprehensive understanding, which are elaborated upon in Appendix C.

### 3.1. Conventional Sliding Surface

SMC allows the system’s dynamic behavior to be tailored by choice of the sliding surface. In terms of tracking, the general sliding surface is defined as a function of tracking errors in the state space  $\mathbb{R}^z$ :

$$\sigma(x, t) = \left(\frac{d}{dt} + \lambda\right)^{z-1} \tilde{x} \tag{7}$$

where the tracking error is defined as  $\tilde{x} = x - x_r$ ;  $\lambda$  is a positive definite diagonal matrix. For a second-order system, Equation (7) is simply a weighted sum of velocity and position errors:

$$\sigma = \dot{\tilde{x}} + \lambda \tilde{x} \tag{8}$$

In direct tracking, the sliding surface and a corresponding proper control yield good performance, as shown in Figure 1a,b in both joint and Cartesian spaces, where a simple 2-DoF manipulator is simulated. It is important to note that to avoid confusion between the x-dimension and the pose of the end-effector in Cartesian space (both typically denoted by 'x'), this paper uses the numerals 1 and 2 to represent the translational dimensions of x and y, respectively. This notation convention will be consistently used in all subsequent figures.

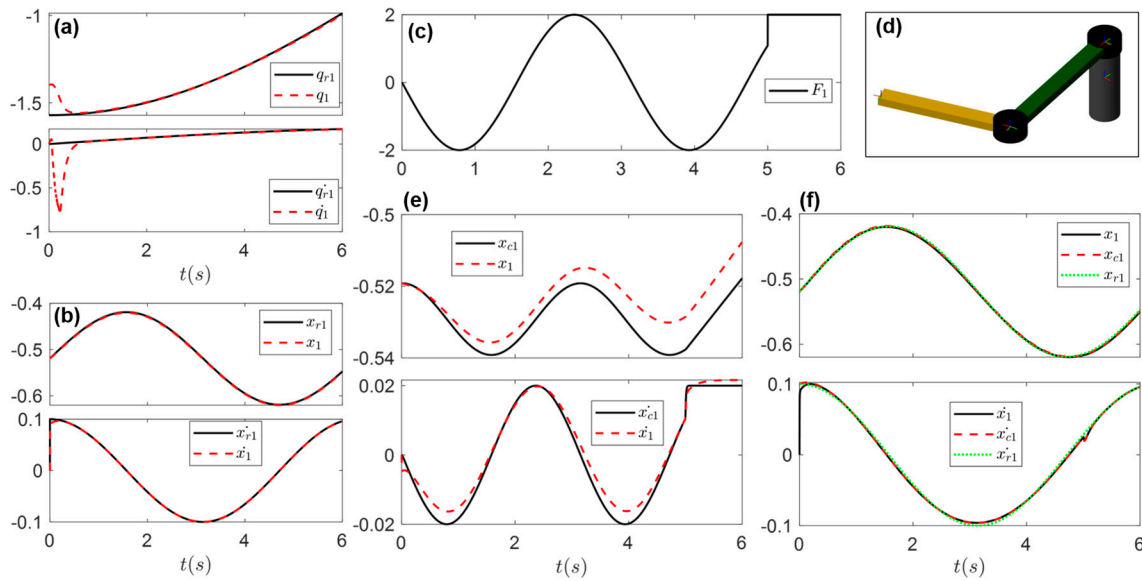


**Figure 1.** Conventional SMC is implemented on a 2-DoF planar manipulator that appeared in (d); (a,b) display direct tracking in joint and Cartesian space, respectively. The reaching phase is observed in (a) when the initial position differs from the reference; (c) displays the interaction force. (e,f) present tracking under admittance control for human-leading and human-following, respectively. In (e), tracking is between actual states and desired response of admittance. In contrast, two tracking goals are required in (f): (i), responses of admittance system track referenced trajectory; (ii), actual trajectory tracks responses of admittance system. Subscription '1' represents the x-axis dimension.

In admittance control, the desired response is computed from Equation (1). SMC is then applied to impose a robust inner tracking control. If the classical approach (i.e., Equation (8)) is applied, then the sliding surface is expressed as

$$\sigma = (\dot{x} - \dot{x}_c) + \lambda(x - x_c) \tag{9}$$

Theoretically, as long as the system states stay on this surface, the desired admittance can be realized via accurate tracking. The sliding surface in Equation (9) was widely adopted in applications of impedance/admittance control [35–37]. The prescribed trajectory and stiffness term were included in admittance in these studies. However, we found that applying Equation (9) gives less accurate results in the human-leading scenario where the targeted admittance is expressed as

$$M_d(t)\ddot{x}_c + D_d(t)\dot{x}_c = f_h \tag{10}$$

The comparison is presented in Figure 1e,f for the robot being a passive follower and a compliant leader, respectively, with the same force profile. In the human-leading case, no reference trajectory is defined, and the tracking is less accurate. In contrast,

accurate tracking for both referenced trajectory and the robot’s desired response in the human-following case is observed.

In fact, the inner controller in human-leading is a velocity controller since Equation (10) is a first-order system. Hence, the sliding surface should be updated as a function of velocity error only according to the definition in Equation (7):

$$\sigma = \dot{x} - \dot{x}_c \tag{11}$$

However, tracking precision is further declined, as shown in Figure 2.

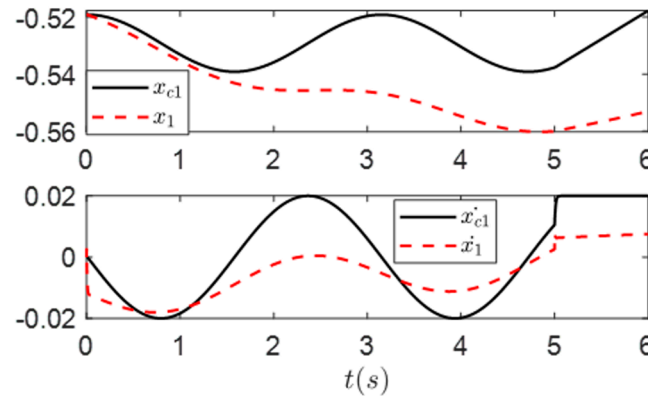


**Figure 2.** SMC for human-leading, where Equation (11) is selected as the sliding surface.

### 3.2. Sliding Surface in Admittance Control

Knowing the limitations of interpreting SMC as direct tracking in realizing desired admittance, a new sliding surface is derived. It is then extended to be a general sliding surface for admittance control.

A rigid manipulator with  $n$ -DoF is considered, and its dynamics, exclusive of friction and uncertainties, are expressed in joint space as

$$H(q)\ddot{q} + C(q, \dot{q})\dot{q} + G(q) = \tau_c + \tau_h \tag{12}$$

where  $q$  denotes the robot’s joint angles, and  $\dot{q}$  and  $\ddot{q}$  represent accelerations and velocities.  $H(q)$  represents a symmetric positive definite inertia matrix;  $C(q, \dot{q})$  is Coriolis and centrifugal matrix;  $G(q)$  is a torque vector generated by gravity;  $\tau_c$  and  $\tau_h$  represents applied torque and external torque, respectively. To adapt to the admittance implemented in the workspace, Equation (12) is written in the Cartesian space as

$$H_w(x)\ddot{x} + C_w(x, \dot{x})\dot{x} + G_w(x) = f_c + f_h \tag{13}$$

where subscript ‘ $w$ ’ represents a fixed Cartesian coordinate at the base of the manipulator in world space, and the mapping from joint to Cartesian space of the end-effector is simply the Jacobian-based operation:

$$\begin{aligned} H_w &= J^{-1T}H(q)J^{-1}, \\ C_w &= -J^{-1T}H(q)J^{-1}\dot{J}J^{-1} + J^{-1T}C(q, \dot{q})J^{-1}, \\ G_w &= J^{-1T}G(q), \\ f_c &= J^{-1T}\tau_c, \\ f_h &= J^{-1T}\tau_h \end{aligned} \tag{14}$$

In [35], the sliding surface was defined as the desired impedance in the integral form. The impedance equation includes system states that are not rigorous unless the perfect tracking (e.g.,  $x = x_c$ ) is assumed. No proof was given in the paper of how to arrive at the suggested control law. In addition, replacing  $\dot{x}$  and  $\ddot{x}$  with the new states (i.e.,  $\dot{x}_s$  and

$\ddot{x}_s$ ), while leaving  $H$ ,  $C$ , and  $G$  as functions of the original system states, is incorrect and creates confusion. A new sliding surface is proposed with theoretical proof to address the above limitations.

Unlike conventional SMC imposing direct tracking, tracking desired response in admittance control can be interpreted as indirect tracking: (i) *realizing desired admittance*; (ii) *tracking desired admittance response*. A sliding surface shall be selected to tailor the dynamic behavior in line with Equation (10), i.e., desired admittance regarding human leading. A straightforward option could be:

$$\sigma = (M_d(t)\ddot{x} + D_d(t)\dot{x} - f_h) - (M_d(t)\ddot{x}_c + D_d(t)\dot{x}_c - f_h) \tag{15}$$

where the precise tracking is assumed, i.e.,  $x = x_c$ . As mentioned,  $x_c$  represents the desired robot response upon human physical interaction. The primary objective of the SMC is to ensure that the robot’s actual response aligns with this desired response. In this context, the assumption facilitates the derivation of a sliding surface and the corresponding control law to achieve this control objective.

Since the sliding surface needs to have at least one relative degree to input  $f_c$ , the integration of Equation (15) is set as the sliding surface for realizing the desired admittance:

$$\sigma = \int (M_d(t)\ddot{x} + D_d(t)\dot{x}) dt - \int (M_d(t)\ddot{x}_c + D_d(t)\dot{x}_c) dt \tag{16}$$

Applying integration by parts to Equation (16) yields

$$\begin{aligned} \sigma &= \left[ M_d(t)\dot{x} - \int \dot{M}_d(t)\dot{x} dt + D_d(t)x - \int \dot{D}_d(t)x dt \right] \\ &\quad - \left[ M_d(t)\dot{x}_c - \int \dot{M}_d(t)\dot{x}_c dt + D_d(t)x_c - \int \dot{D}_d(t)x_c dt \right] \end{aligned} \tag{17}$$

Taking time derivative to Equation (17) obtains

$$\begin{aligned} \dot{\sigma} &= \left[ \dot{M}_d(t)\dot{x} + M_d(t)\ddot{x} - \dot{M}_d(t)\dot{x} + \dot{D}_d(t)x - D_d(t)\dot{x} - \dot{D}_d(t)x \right] \\ &\quad - \left[ \dot{M}_d(t)\dot{x}_c + M_d(t)\ddot{x}_c - \dot{M}_d(t)\dot{x}_c + \dot{D}_d(t)x_c - D_d(t)\dot{x}_c - \dot{D}_d(t)x_c \right] \\ &= M_d(t)\ddot{x} + D_d(t)\dot{x} - M_d(t)\ddot{x}_c - D_d(t)\dot{x}_c \end{aligned} \tag{18}$$

To obtain equivalent control, we set  $\dot{\sigma} = 0$ , which yields

$$M_d(t)\ddot{x} + D_d(t)\dot{x} - M_d(t)\ddot{x}_c - D_d(t)\dot{x}_c = 0 \tag{19}$$

Solving Equation (13) for  $\ddot{x}$  and substituting into Equation (19) gives the equivalent control as

$$u_{eq} = H_w(x) \left( \ddot{x}_c + M_d^{-1}(t)D_d(t)\dot{x}_c - M_d^{-1}(t)D_d(t)\dot{x} \right) + C_w(x, \dot{x})\dot{x} + G_w(x) - f_h \tag{20}$$

Equation (19) can further be simplified by substituting  $\ddot{x}_c$  solved from Equation (10) as

$$u_{eq} = H_w(x) \left( -M_d^{-1}(t)D_d(t)\dot{x} - M_d^{-1}(t)f_h \right) + C_w(x, \dot{x})\dot{x} + G_w(x) - f_h \tag{21}$$

It is important to note that the term  $\left( -M_d^{-1}(t)D_d(t)\dot{x} + M_d^{-1}(t)f_h \right)$  is nothing but the double integrator in feedback linearization of Equation (13) with

$$\ddot{x} = v \tag{22}$$

and

$$v = -M_d^{-1}(t)D_d(t)\dot{x} + M_d^{-1}(t)f_h \tag{23}$$

where  $v$  is known as the new input. Substituting Equation (23) into (18) arrives at

$$\dot{\sigma} = -M_d(t)\ddot{x}_c + -D_d(t)\dot{x}_c + f_h \tag{24}$$

The right side of Equation (24) is exactly the targeted admittance and is always equal to zero. Equation (24) is exactly the targeted admittance and is always equal to zero. It also suggests that Equation (18) is equal to zero with the unique solution,  $\dot{x} = \dot{x}_c$ . Thus, it also allows satisfaction of the second goal: tracking desired admittance response. That being the case, Equation (22) can be defined as an equivalent acceleration signal:

$$\ddot{x}_s = -M_d^{-1}(t)D_d(t)\dot{x} + M_d^{-1}(t)f_h \tag{25}$$

Notice that the above equation represents perfect tracking of desired admittance response if  $\ddot{x}_s = \ddot{x}$ . Then, a new sliding surface is defined as

$$\sigma = \dot{x} - \dot{x}_s \tag{26}$$

It has a relative degree of one regarding control input, which can be seen from

$$\dot{\sigma} = \ddot{x} - \ddot{x}_s \tag{27}$$

It is interesting to note that the desired response of the robot, i.e.,  $\dot{x}_c$ , does not explicitly appear in the control loop but is tracked by actual system states. The above derivation is also valid and satisfied in the human-following case (refer to Appendix A for more details). One of the main advantages of the new method is that the sliding surface is universal in both human-leading and human-following cases, regardless of the order of the desired admittance.

Simulation results of using the new sliding surface appear in Figure 3. In comparison to Figure 1e, a noticeable improvement is observed in tracking accuracy. In addition, the good performance in both cases suggests that the new sliding surface is independent of the order of the desired admittance system.

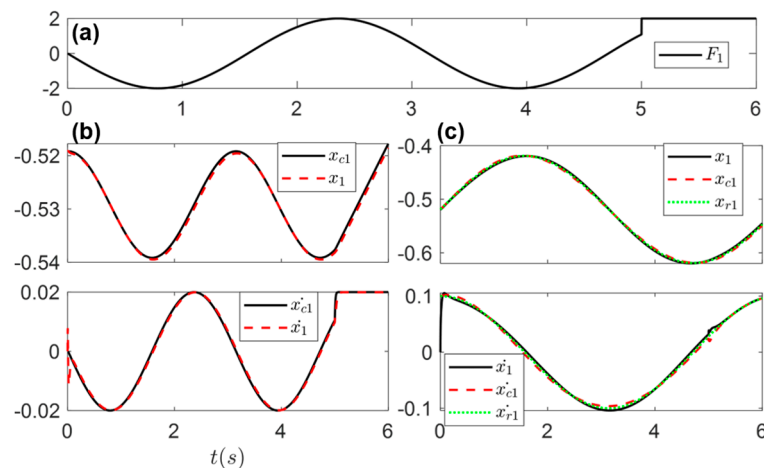


**Figure 3.** SMC with the new sliding surface being applied: (a) displays the same force profile in Figure 1. Admittance response,  $x_c$ , does not explicitly appear in the controller; nonetheless, it is tracked by actual states accurately. In comparing (b) to Figure 1e, an improvement is observed that suggests the efficiency of the proposed method. Moreover, the same sliding surface works well for both human-leading and human-following cases as appeared in (c).

### 3.3. Reachability in VAC

In general, there are two steps involved in SMC design: defining a sliding surface to satisfy desired dynamic behavior and designing a controller to drive system states to stay on the sliding surface. As seen in the previous section, selecting a sliding surface for

admittance control was completed. This section aims to prove the sufficient condition (or reachability condition) for ensuring sliding mode in VAC.

Previous studies have proven the reachability of conventional SMC in the sense of Lyapunov [35–37]. However, the proof is based on a 2-DoF system where the analytical expression of Coriolis and centrifugal matrix can be uniquely determined, such that the skew-symmetric property of  $\dot{H}_w - 2C_w$  is valid in this case. For a higher DoF system,  $C_w$  has infinite solutions. Only a specific definition of  $C_w^*$  (Chapter 9 in [33]) satisfies  $\dot{H}_w = C_w^* + C_w^{*T}$ , that is

$$C_{ij} = \frac{1}{2} \dot{H}_{ij} + \frac{1}{2} \sum_{k=1}^n \left( \frac{\partial H_{ik}}{\partial x_j} - \frac{\partial H_{jk}}{\partial x_i} \right) \dot{x}_k \tag{28}$$

In order to prove the stability of a controller, the analytical model of robot dynamics is required. This analytical model is usually obtained via the Euler-Lagrange method and yields

$$H_w(x)\ddot{x} + S_w(x, \dot{x}) + G_w(x) = f_c + f_h \tag{29}$$

where  $S_w(x, \dot{x})$  is Coriolis and centrifugal force. And factorization of  $C_w$  by  $S_w$  is not unique. A problem then naturally arises: How does the proof using a specific solution of  $C_w$ , i.e.,  $C_w^*$ , guarantee overall reachability for all solutions of  $C_w$ ? To address this issue, the unique  $S_w(x, \dot{x})$  is adopted, and the term  $C_w^*$  is modeled as a source of uncertainty (refer to the following proof). Furthermore, time-varying admittance parameters are taken into account.

**Control law for SMC in VAC.** The system is stable in the sense of Lyapunov with the control law considering uncertainties and disturbances:

$$u = \hat{H}_w(x)\ddot{x}_s + \hat{S}_w(x, \dot{x}) + \hat{G}_w(x) - \Delta - f_h - K_{smc} \text{sign}(\sigma) \tag{30}$$

where

$$K_{smc} \geq \delta_H \| \ddot{x}_s \| + \delta_S + \delta_G + \delta + \eta \tag{31}$$

and,

$$\| \ddot{x}_s \| \leq \frac{\lambda(D_{max})}{\lambda(M_{min})} \| \dot{x} - \dot{x}_r \| + \frac{\lambda(K_{max})}{\lambda(M_{min})} \| x - x_r \| \tag{32}$$

where  $\delta_H$ ,  $\delta_S$ , and  $\delta_G$  denote the bounds of uncertainties of dynamic modeling, and  $\delta$  represents the approximate bounds of uncertainties from other resources. In Equation (30),  $\hat{H}_w$ ,  $\hat{S}_w$ , and  $\hat{G}_w$  represent the approximation of dynamic modeling;  $K_{smc}$  denotes the sliding mode gain; other uncertainties, for example, unmodeled friction force, computational errors, and  $C_w^*$  term (will appear in Equation (39)) are assigned to  $\Delta$ .

**Proof.** A Lyapunov candidate function is selected as

$$V(\sigma) = \frac{1}{2} \sigma^T H_w \sigma \tag{33}$$

Taking the time derivative of Equation (33) arrives at

$$\dot{V}(\sigma) = \sigma^T H_w \dot{\sigma} + \frac{1}{2} \sigma^T \dot{H}_w \sigma \tag{34}$$

Assuming  $C_w = C_w^*$  that satisfies  $\dot{H}_w(x) - 2C_w^*(x, \dot{x})$  leads to

$$\dot{V}(\sigma) = \sigma^T H_w \dot{\sigma} + \sigma^T C_w^* \sigma \tag{35}$$

Substitution of Equation (26) into Equation (35) results in

$$\begin{aligned} \dot{V}(\sigma) &= \sigma^T \left( H_w \ddot{x} - H_w \ddot{x}_s + C_w^* \dot{x} - C_w^* \dot{x}_s \right) \\ &= \sigma^T \left( f_c + f_h - G_w - H_w \ddot{x}_s - C_w^* \dot{x}_s \right) \end{aligned} \tag{36}$$

where  $f_c$  is the control input  $u$ . According to  $\dot{\sigma} = 0$  in Equation (27), the equivalent control can be derived as

$$u_{eq} = \hat{H}_w(x) \ddot{x}_s + \hat{S}_w(x, \dot{x}) + \hat{G}_w(x) - \Delta - f_h \tag{37}$$

The approximation of dynamic modeling is assumed to obey the following inequalities.

$$\begin{aligned} \|\Delta H_w(x)\| &= \|\hat{H}_w(x) - H_w(x)\| \leq \delta_H, \\ \|\Delta S_w(x, \dot{x})\| &= \|\hat{S}_w(x, \dot{x}) - S_w(x, \dot{x})\| \leq \delta_S, \\ \|\Delta G_w(x)\| &= \|\hat{G}_w(x) - G_w(x)\| \leq \delta_G \end{aligned} \tag{38}$$

where the norm operator represents the Euclidean norm. Analytical solutions of  $\hat{H}_w(x)$ ,  $\hat{S}_w(x)$ , and  $\hat{G}_w(x)$  include kinematic parameters and inertial terms. As long as the modeling uncertainties are bounded, the above assumption is valid. Substituting Equations (37) and (38) into Equation (36) arrives

$$\dot{V}(\sigma) = \sigma^T \left( \Delta H_w \ddot{x}_s + \Delta S_w + \Delta G_w + C_w^* \sigma + \Delta - K_{smc} \text{sign}(\sigma) \right) \tag{39}$$

For an exact dynamic model of the robot,  $C_w^*$  is bounded as long as the entire system is stable. Moreover,  $\sigma$  is also bounded and approaches zero. Therefore, it is fair to assume that  $C_w^* \sigma$  is bounded, such that it can be modeled as bounded uncertainty. To this end, Equation (39) is reduced to

$$\dot{V}(\sigma) = \sigma^T \left( \Delta H_w \ddot{x}_s + \Delta S_w + \Delta G_w + \Delta - K_{smc} \text{sign}(\sigma) \right) \tag{40}$$

As a result, no analytical solution of  $C_w$  is required in the proof process. Applying inequality property of the inner product and norm (i.e.,  $\langle a, b \rangle \leq \|a\| \|b\|$ ) and the property of  $\|a \cdot b\| \leq \|a\| \|b\|$  to Equation (40), one gets

$$\dot{V} \leq \|\sigma\|^T \left( \delta_H \|\ddot{x}_s\| + \delta_S + \delta_G + \delta - K_{smc} \right) \tag{41}$$

Substituting Equation (31) into Equation (40), the well-known  $\eta$ -reachability condition [33],  $\dot{V} \leq -\eta \|\sigma\|$ , is satisfied.

For variable admittance system, the extreme values of admittance parameters are assumed to be known. Then, the following inequalities are assumed:

$$\begin{aligned} \frac{1}{\lambda(M_{max})} &\leq \|M_d(t)^{-1}\| \leq \frac{1}{\lambda(M_{min})}, \\ \lambda(D_{min}) &\leq \|D_d(t)\| \leq \lambda(D_{max}), \\ \lambda(K_{min}) &\leq \|K_d(t)\| \leq \lambda(K_{max}) \end{aligned} \tag{42}$$

Taking the Euclidean norm of Equation (A7) (refer to Appendix A) with the definition of  $A = \ddot{x}_r + M_d^{-1} f_h$  and  $B = M_d^{-1} D_d (\dot{x} - \dot{x}_r) + M_d^{-1} K_d (x - x_r)$ , and applying the inequality property  $\|A - B\| \geq \|A\| - \|B\|$  results in

$$\|\ddot{x}_s\| \geq \|A\| - \|B\| \tag{43}$$

Simplifying the above equation gives

$$\|\ddot{x}_s\| \leq \|B\| - \|A\| \tag{44}$$

By substituting *A* and *B* in the above equation, one obtains

$$\|\ddot{x}_s\| \leq \frac{\lambda(D_{max})}{\lambda(M_{min})} \|(\dot{x} - \dot{x}_r)\| + \frac{\lambda(K_{max})}{\lambda(M_{min})} \|x - x_r\| - \frac{1}{\lambda(M_{min})} \|f_h\| - \|\ddot{x}_r\| \quad (45)$$

and

$$\|\ddot{x}_s\| \geq \frac{1}{\lambda(M_{min})} \|f_h\| + \|\ddot{x}_r\| - \frac{\lambda(D_{max})}{\lambda(M_{min})} \|(\dot{x} - \dot{x}_r)\| - \frac{\lambda(K_{max})}{\lambda(M_{min})} \|x - x_r\| \quad (46)$$

Then, a more conservative bound in terms of system stability, i.e., Equation (32), is obtained that further proves the reachability condition. □

In the following discussion, a relatively large modeling error in the mass of each link is intentionally introduced to investigate system robustness and stability. Analytical expressions for  $H_w$ ,  $S_w$ , and  $G_w$  incorporated the mass of every link in the manipulator. Subsequently, the threshold values in Equation (38) were determined to maintain consistency in position and velocity while varying the mass values. In both simulation and experimental validation, a higher sliding mode gain was employed to ensure system stability and responsiveness in the face of other uncertainties. It is crucial to note that in real-world scenarios, the sliding mode gains and other control parameters must be meticulously calibrated, considering the unique demands of the given task. The primary goal of this research is to establish foundational knowledge for the robust and precise application of the proposed sliding mode control law in variable admittance control.

The proposed controller is implemented in SIMULINK (MathWorks, Inc. 2022, Natick, MA, USA). The 7-DoF Kinova Gen3 (Kinova, Inc., Boisbriand, QC, Canada) with a Robotiq FT-300 force sensor (Robotiq, Lévis, QC, Canada) is modeled using Simscape Multi-body(MathWorks, Inc. 2022, Natick, MA, USA) for the closest simulation to reality. The system is then modeled as a planar ( $n = 2$ ) 3-DoF configuration in Figure 4a, where joints 1, 4, and 6 are activated. Linear motion is of interest for analyzing the system behaviors; hence, high admittance parameters are selected for the rotational motion to allow orientation of the end effector of the robot to have no significant change during the interaction. In addition, a robust damped least-squares method [45,46] is applied in case the system becomes unstable near or at singularity configuration ( $0^\circ$  of joint 4).

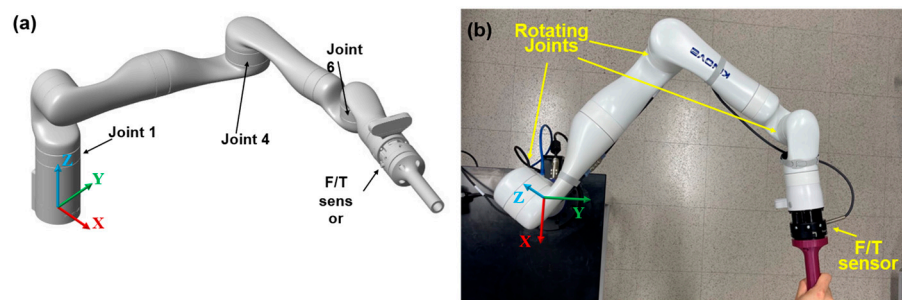


**Figure 4.** (a) Simulink model of the manipulator under a planar 3-DoF configuration and (b) Physical human–robot interaction scene with an experimental setup that has a similar configuration.

The proposed control law allows system states to be in sliding mode even in the presence of time-varying admittance parameters. Comparing the results in Figure 5, the method in the literature [35–37] is insufficient to tackle VAC, while our approach not only ensures relatively accurate tracking but also demonstrates robustness. The robustness can be seen from three aspects: (i) the modeling error is designed to be large; (ii) the numerical solver adopts 1st-order Newton methods; (iii) and  $C_w^*$  term is modeled as a bounded uncertainty. In addition, the human-intention-based VAC is realized. Equation (5) allows for the maximum allowable operation velocity to be constrained within 0.1 m/s. According

to the effort-saving law in Equation (2), the velocity is maintained even if the applied force restores to the nominal level between 5–6 s (from  $-7$  N to  $-5$  N).

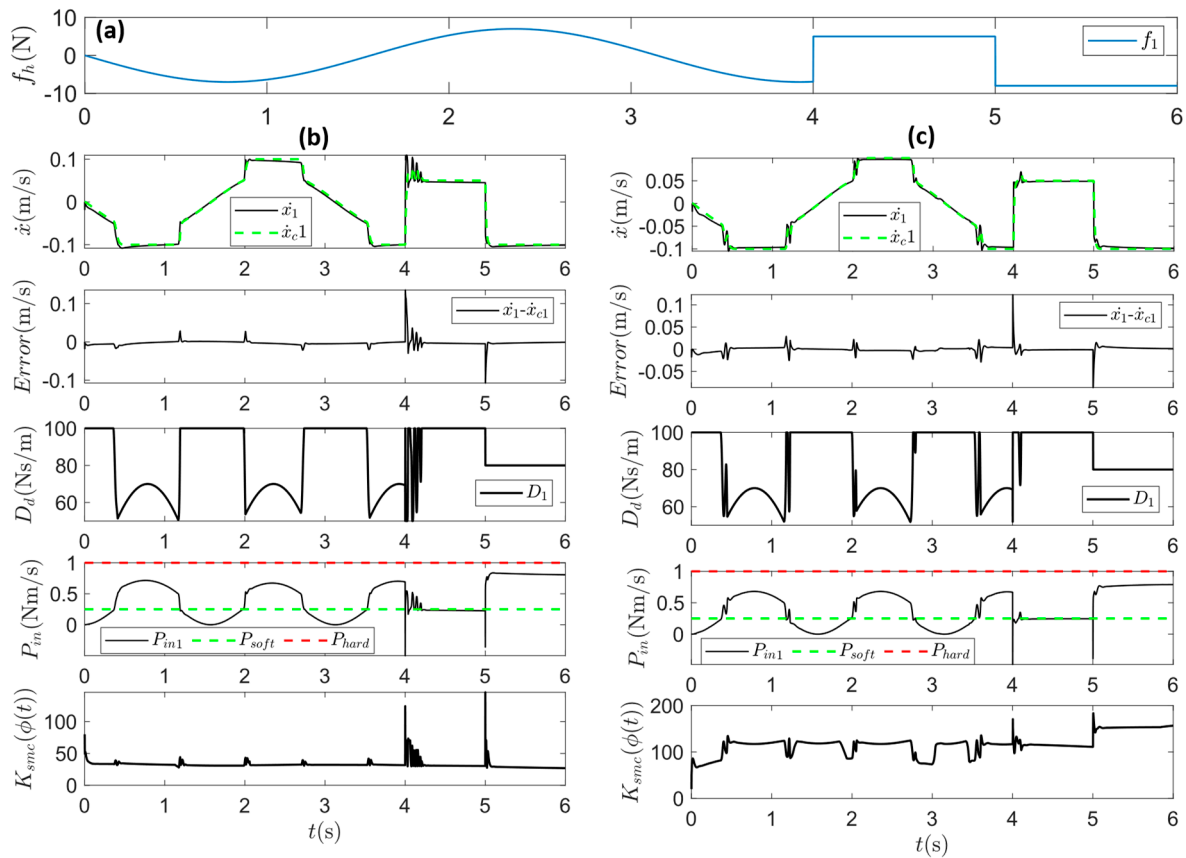


**Figure 5.** Implementation of SMC in VAC for Kinova Gen3. (a) displays the interaction force. The nominal force in Equation (2) is defined as 5 N, and the maximum safe operating speed is selected as 0.1 m/s in Equation (5). Effort-saving behavior is reflected by the observation that higher velocity is maintained even if the interaction force restores the nominal level from  $-7$  N between 4–5 s. Safe interaction is reflected by the constrained velocity within 0.1 m/s under higher force. In (b), a sliding mode gain is used without considering time-varying admittance parameters, resulting in oscillation around 4 s. In contrast, the proposed control law, i.e., Equations (30)–(32), leads to an improvement in performance in (c). The modeling error is purposely designed to be large to demonstrate the robustness of the controller, where the mass of each link in modeling is designed as  $\hat{m}_1 = 0.93$  kg,  $\hat{m}_2 = 0.27$  kg, and  $\hat{m}_3 = 60$  kg, compared to the exact value,  $m_1 = 9.3$  kg,  $m_2 = 2.7$  kg, and  $m_3 = 6.0$  kg, respectively.

### 3.4. Chattering Removal

The proposed control law consists of discontinuous control that usually gives rise to chattering. One of the most used techniques to reduce chattering is replacing the signum function in Equation (30) with a saturation function,  $sat(s_i/\epsilon)$ ,

$$sat\left(\frac{\sigma_i}{\phi_i}\right) = \begin{cases} 1, & \sigma_i/\phi_i > 1 \\ \sigma_i/\phi_i, & -1 < \sigma_i/\phi_i < 1 \\ -1, & \sigma_i/\phi_i < -1 \end{cases} \quad (47)$$

It compromises stability and tracking precision to a certain degree by adding a boundary layer with a thickness of  $\phi_i$  ( $i = 1 \dots n$ ) to the sliding surface. One disadvantage of the above technique is that  $\phi_i$  needs to be designed by trial and error to achieve a trade-off

between robustness and tracking precision. For example, the chattering appears in Figure 6 (c.f., Figure 5c) if the boundary layer thickness is too small.

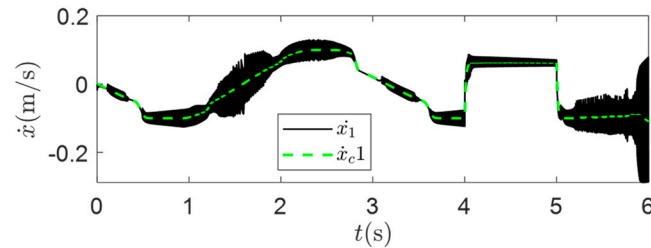


**Figure 6.** Chattering phenomenon is observed when boundary layer thickness is decreased from 0.1 in Figure 5c to 0.03.

In [33],  $\phi_i$  was made time-varying for exploiting the control bandwidth:

$$\dot{\phi}_i(t) + \lambda_i \phi_i(t) = K_{smc}^0(x_s) \tag{48}$$

where  $K_{smc}^0$  indicates the initial value of sliding mode gain computed from Equation (30);  $\lambda_i$  shares the same definition as appeared in Equation (8); it can be recognized as the break-frequency in the first-order filter of input perturbations (or uncertainties) to output  $\sigma$ . Then  $K_{smc}$  can be defined as a function of boundary layer thickness as

$$K_{smc} = K_{smc}(x) - K_{smc}(x_s) + \lambda_i \phi_i(t) \tag{49}$$

The merit of the time-varying boundary layer is that it takes system uncertainties into account, such that its thickness is adapted to system dynamic changes. Though,  $K_{smc}(x)$  and  $K_{smc}(x_s)$  might have deviations at the beginning of the reaching phase, in which  $x \neq x_s$ , considering the finite reach time of sliding mode control and subtraction in Equation (49), it is fairly assumed  $K_{smc}(x) \approx K_{smc}(x_s)$  during the sliding mode under constraints of boundary layer. As a result, one obtains

$$K_{smc} = \lambda_i \phi_i \tag{50}$$

Combining Equations (46) and (48) in the Laplace domain, one obtains

$$\mathcal{L}(K_{smc}) = \frac{\lambda \mathcal{L}(K_{smc}^0)}{s + \lambda} \tag{51}$$

$K_{smc}$  is nothing but a low-pass-filtered version of  $K_{smc}^0$ . In our case  $K_{smc}^0$  is calculated from Equation (31), which guarantees system stability. In fact, the definition of Equation (31) considers the worst-case scenario, i.e.,  $\|\ddot{x}_s\|$  is maximized in the presence of bounded uncertainties. Hence, the new low-pass-filtered gain does not distort the stability condition. It is crucial to notice that our sliding surface, i.e., Equation (26), does not include  $\lambda$ . In our definition, it is a virtual term used to tune the filter-like structure. The rule of thumb for selecting  $\lambda$  is  $\lambda \approx \frac{1}{4}f$ , where  $f$  is the sampling rate. The performance appears in Figure 7. It yields good performance in achieving a trade-off between chattering removal and robustness.

### 3.5. Acceleration Feedback in SMC

In Figure 7, the overshooting phenomenon is observed. One reason could be that the limited bandwidth of the system results in a delayed reaction. Therefore, this section introduces acceleration feedback to improve control performance.

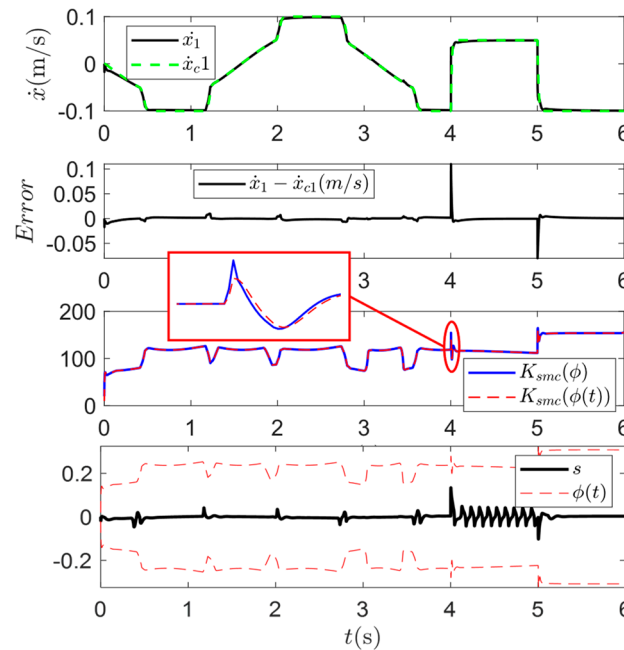


**Figure 7.** The variable boundary layer approach is applied in implementing SMC in VAC, in which the same VAC models and force profile are employed as in Figure 5c. Tracking is relatively accurate, and the boundary layer thickness does not need to be defined by trial and error. It is also observed that the new sliding mode gain is simply a low-pass filtered signal of Equation (31). The modeling errors are designed the same as in Figure 5.

The equivalent control is interpreted as the continuous control that maintains system motion restricted to the sliding mode in the absence of disturbances and uncertainties. It consists of exact system dynamics (best approximation). Therefore, we include acceleration error,  $\ddot{\tilde{x}} = \ddot{x} - \ddot{x}_s$ , in the equivalent control such that the bandwidth of system can be influenced (i.e., increased),

$$u_{eq} = \hat{H}_w \ddot{x}_s + \hat{S}_w + \hat{G}_w - \Delta - f_h - \hat{H}_w Q \ddot{\tilde{x}} \tag{52}$$

where  $Q$  is a positive definite dynamic matrix gain. Since the equivalent control is obtained by setting  $\dot{\sigma} = 0$ , then a new sliding surface shall be derived inversely to adapt to the introduced acceleration feedback. However, it is learned that Equation (26) also satisfies SMC with acceleration feedback. Derivation in Appendix B shows that adding the acceleration feedback does not change the stability of the original system. The extended system bandwidth could explain the improved performance in tracking and robustness against uncertainties [40–43]. In fact, the way the acceleration error feeds into the control loop in the present paper is similar to what has been studied as a Plug-in structure in [41]. It has been shown that acceleration has no impact on stability conditions in this structure.

In the end, numerical simulation is conducted by compiling the proposed approaches in Section 3 together, yielding results shown in Figure 8. Comparing Figures 7 and 8b, it concludes that adding acceleration feedback results in smooth and perfect tracking in the presence of significant uncertainties. In addition to the robot acting as a passive follower, our approach performs well in human-following cases. A sinusoidal trajectory,  $x_r$ , is prescribed and tracked by the robot to provide physical support to the human. Assuming the interaction is normal and safe (recall the human intention framework in Section 2), human interaction is recognized as a disturbance. The stiffness is increased proportional to the human’s applied force, then regulated by PER. The proposed SMC not only ensures the tracking between  $x_c$  and  $x_r$  but also between  $x$  and  $x_c$ .

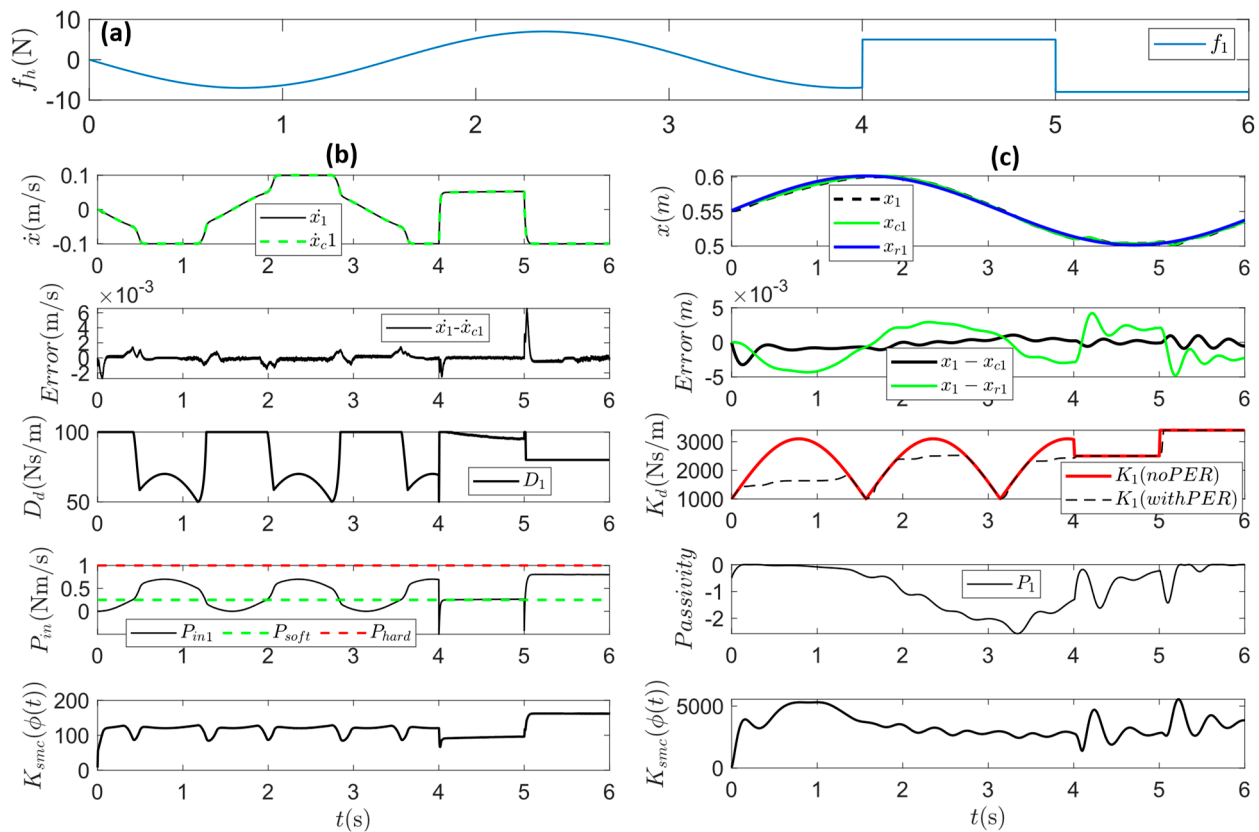


**Figure 8.** Implementation of SMC in VAC for Kinova Gen3, where acceleration feedback is included. (a) displays the interaction force. (b) illustrates the control in human leading case. A smooth and perfect tracking is observed compared to Figure 5b. In (c), stiffness is updated proportional to the human interaction force, then is regulated by PER. As a result, system passivity is preserved, i.e.,  $\frac{1}{2} \dot{K}_d^i(t) \tilde{x}_i^2 \leq \mu D_d^i \tilde{x}_i^2$ . Moreover, tracking of  $x_r$  by  $x_c$  and  $x_c$  by  $x$  are both realized. The modeling errors are designed the same as in Figure 5.

#### 4. Experimental Validation

Experiments are conducted on a 7-DoF manipulator, Kinova Gen3, with the above-proposed control models implemented. The same 3-DoF configuration described earlier in Figure 4a is adopted. The user grabs the handle to move the robot in the x-y plane, and the motion is random on the premise of avoiding kinematic singularity. For the kinematic and dynamic parameters (1) the length and mass of each link of the manipulator are referred to values in the user manual of Kinova Gen3; (2) the length and mass of F/T sensor and handle are measured and included; (3) the center of mass and moment of inertia are roughly approximated.

The conventional SMC for VAC in human-leading is implemented first. In this case, the sliding mode gain and boundary layer thickness are constants, and no acceleration feedback is included. For admittance control, the proposed variable damping model and PER are applied. In the initial test,  $K_{smc}^i$  and  $\phi_i$  is selected as 20 and 0.1, respectively. The actual mass of each link is applied in the dynamic model, where  $m_1 = 3.70$  kg,  $m_2 = 1.61$  kg, and  $m_3 = 1.75$  kg. Link 1 is proximal to the manipulator base, and link 3 is the distal link. It is observed in Figure 9 that tracking is relatively accurate during acceleration and deceleration phases but less accurate in tracking the desired response under the constraint of maximum allowed velocity, 0.1 m/s. It is essential to clarify the difference between the actual link mass of the physical manipulator used here and those values in simulation (c.f. Figure 5). The link mass of manipulator in the Simscape model is extracted from the 3D model provided by Kinova, while the mass of the physical link is from the user manual.

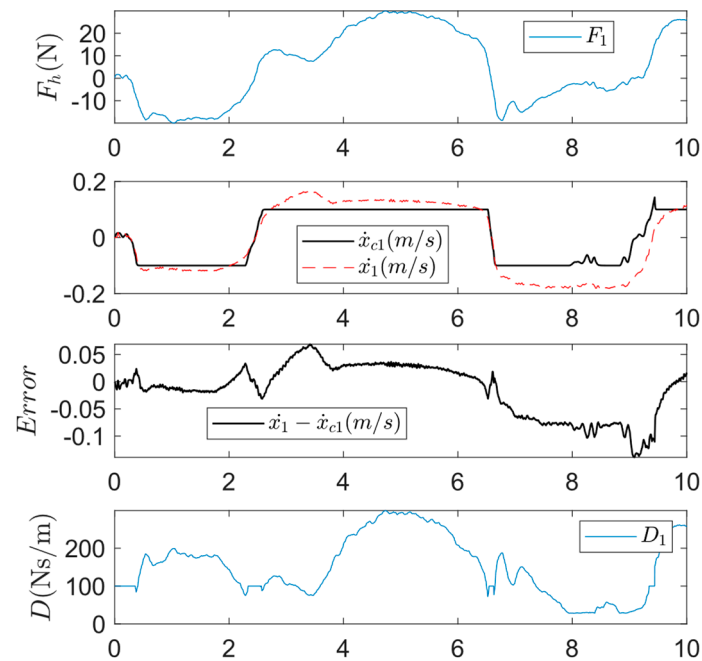


**Figure 9.** Tracking performance of applying indirect tracking approach for human-leading VAC with a constant sliding mode gain,  $K_{smc}^i = 20$ .

Then, the same algorithm is applied with a higher sliding mode gain,  $K_{smc}^i = 70$ , which yields results as shown in Figure 10. Though the tracking accuracy is improved from the perspective of the dominant trend of actual velocity, the oscillatory signal indicates that the selected gain value is too high. It is experimentally verified that optimizing the trade-off between tracking accuracy and vibration-free motion for the conventional method in dealing with VAC is practically difficult.

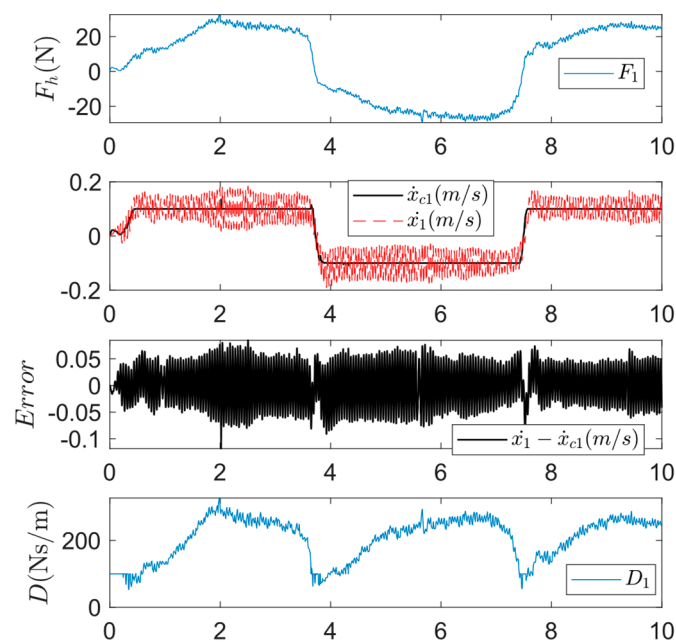


**Figure 10.** Tracking performance of applying indirect tracking approach for human-leading VAC with a constant sliding mode gain,  $K_{smc}^i = 70$ .

The robustness test is then conducted by reducing the mass of link 1 and link 3 to be  $m_1 = 2.3$  kg and  $m_3 = 0.65$  kg in the dynamic equation, where  $K_{smc}^i = 20$ . As expected, tracking performance is further degraded, as appears in Figure 11, due to the constant sliding mode gain insufficiently tackling the included modeling uncertainties.

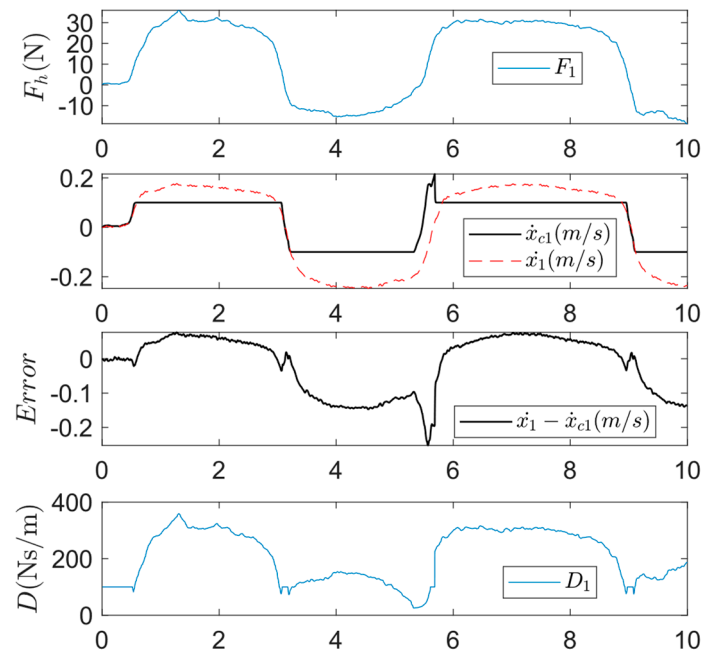


**Figure 11.** Tracking performance of applying indirect tracking approach for human-leading VAC with a constant sliding mode gain,  $K_{smc}^i = 20$ . The mass of links 1 and 3 are modified to be  $m_1 = 2.3$  kg and  $m_3 = 0.65$  kg in the controller.

Then, the variable boundary layer thickness (or variable sliding mode gain) approach is applied to address the above issue. The robustness test is also included where the mass of links 1 and 3 are modified to be  $m_1 = 2.3$  kg and  $m_3 = 0.65$  kg in the dynamic model, which yields results in Figure 12. The tracking accuracy is improved, and the vibration is attenuated. Nonetheless, the overshooting phenomena are observed when actual velocity hits the constraint.

To investigate if including acceleration feedback can resolve the above issue, the proposed control algorithm in Equation (52) is implemented. Considering the operational safety when feeding a noisy acceleration signal back to the control loop, a small gain is selected at the initial test, i.e.,  $Q_i = 3.0$ . Again, the same modeling errors, i.e.,  $m_1 = 2.3$  kg and  $m_3 = 0.65$  kg, on link mass are included to examine the controller's robustness. The built-in accelerometer measures acceleration at the endpoint of manipulator. The results appear in Figure 13. As expected, the overshooting is appropriately attenuated. However, an oscillatory signal is observed and is not favorable. The reason could be the resonance between high-frequency unstructured dynamics and the noisy acceleration signal.

To obtain smooth acceleration data with less distortion and phase lag, a structure composed of a second-order low-pass filter and a modified parabolic sliding mode filter (M2-PSMF) (refer to [43]) is applied to the measured acceleration as well as equivalent acceleration (i.e.,  $\ddot{x}_s$ ). With the filter being applied, tracking performance is promoted, as shown in Figure 14. Also, no high-magnitude overshooting signal is observed. The decent results that match the simulation results in Figure 8a demonstrate the proposed controller's effectiveness and robustness. The performance of the filter is shown in Figure 15.

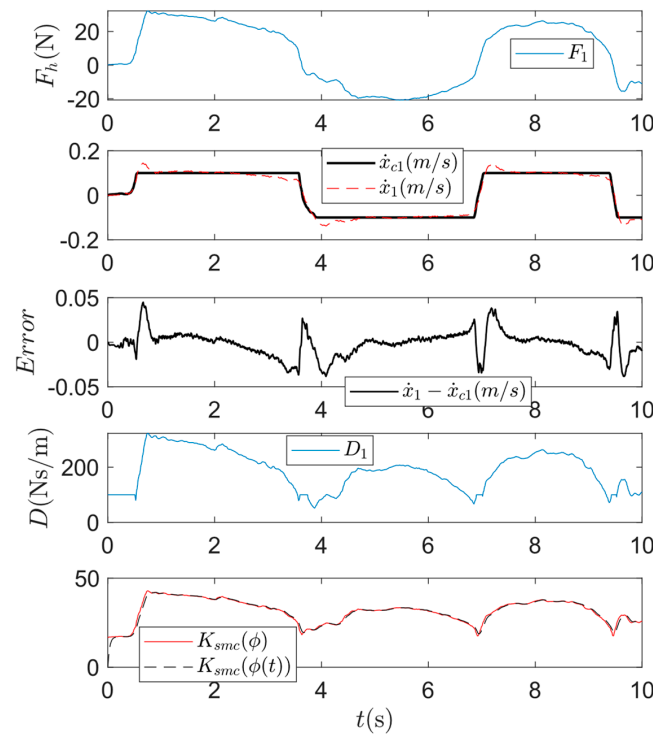


**Figure 12.** Tracking performance of applying indirect tracking approach without AFC for human-leading VAC. The proposed variable sliding mode gain and variable boundary layer thickness methods are employed. The mass of links 1 and 3 are modified to be  $m_1 = 2.3$  kg and  $m_3 = 0.65$  kg in the controller.

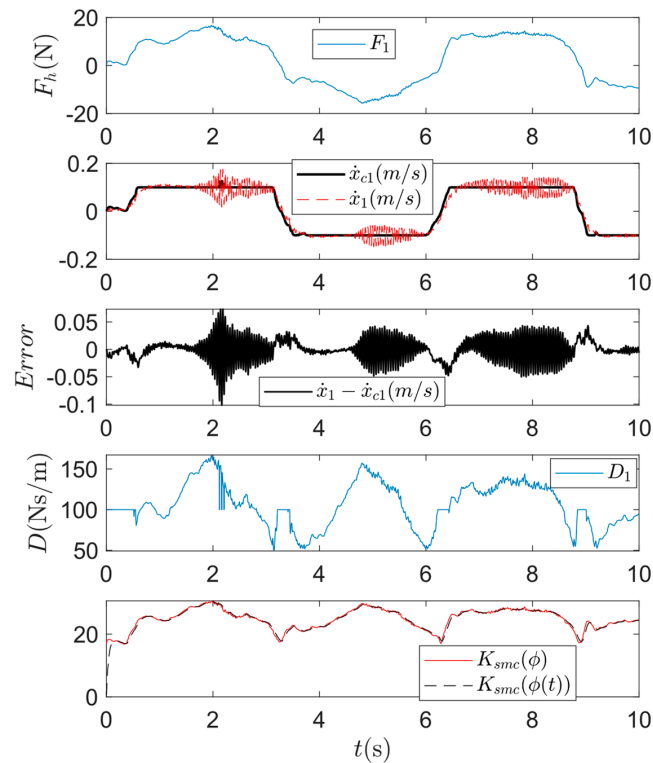


**Figure 13.** Tracking performance of indirect tracking approach with AFC for human-leading VAC. The proposed variable sliding mode gain and variable boundary layer thickness methods are employed. Acceleration error gain is selected as  $Q_i = 3.0$ . The mass of links 1 and 3 are modified to be  $m_1 = 2.3$  kg and  $m_3 = 0.65$  kg in the controller.

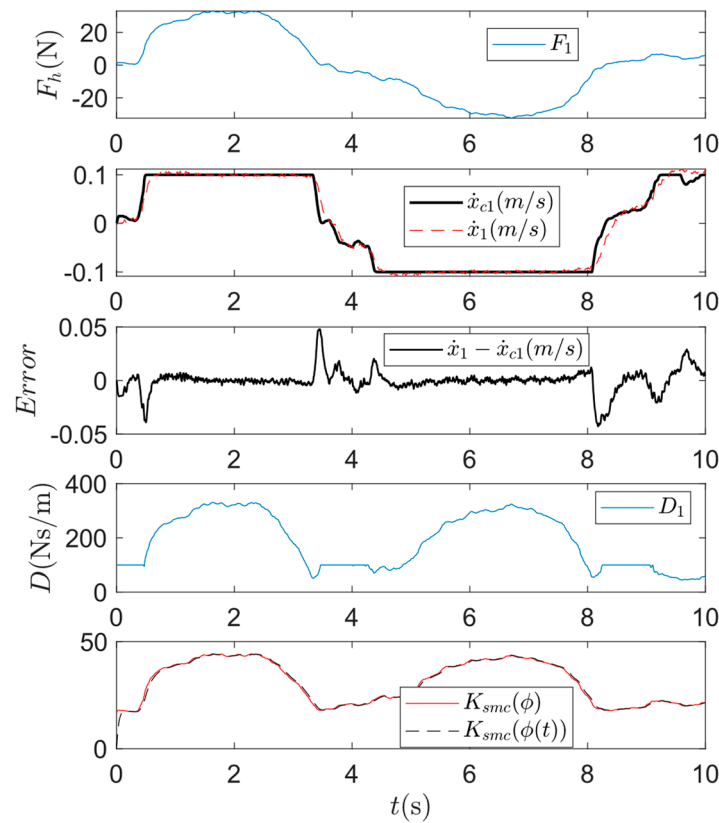


**Figure 14.** Tracking performance of indirect tracking approach with AFC for human-leading VAC. The proposed variable sliding mode gain and variable boundary layer thickness methods are employed. The structure composed of a second-order low-pass filter and M2-PSMF filter is applied to acceleration signals. Acceleration error gain is selected as  $Q_i = 3.0$ . The mass of links 1 and 3 are modified to be  $m_1 = 2.3$  kg and  $m_3 = 0.65$  kg.

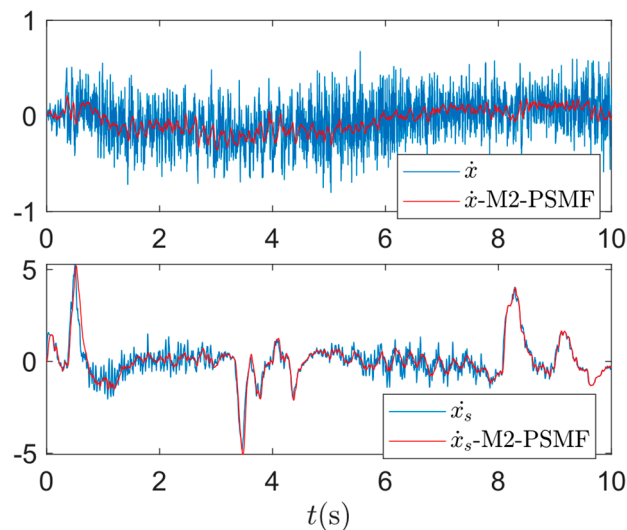


**Figure 15.** Filtered measured acceleration and equivalent acceleration signals using the M2-PSMF filter.

Furthermore, to verify the robustness of the proposed overall control law when the modified mass is greater than the actual value, the mass of link 3 is changed to 2.75 kg in the model. Accurate tracking performance appears in Figure 16.

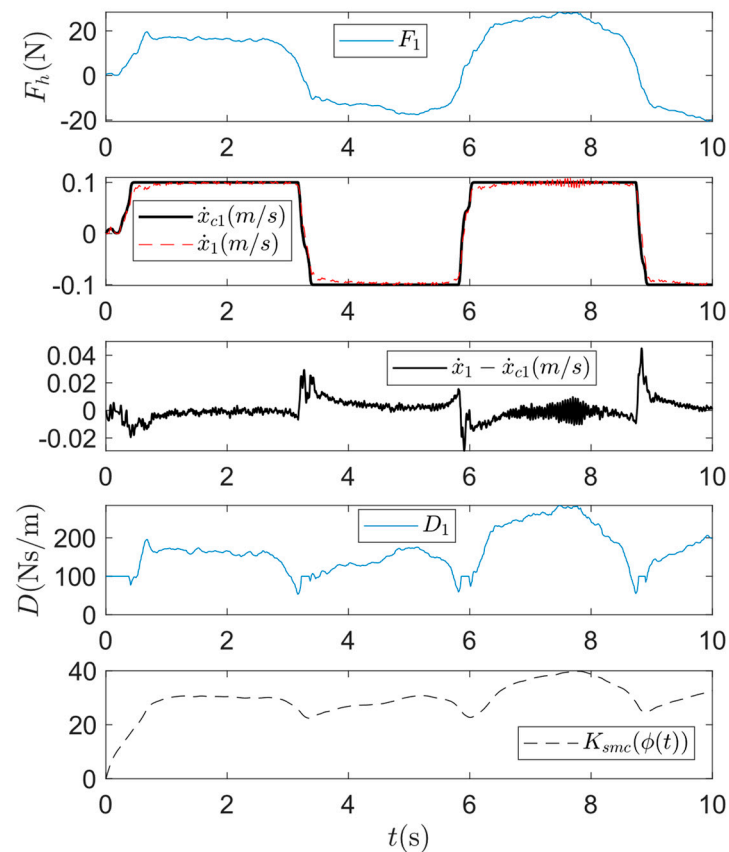


**Figure 16.** Tracking performance of indirect tracking approach with AFC for human-leading VAC. The proposed variable sliding mode gain and variable boundary layer thickness methods are employed. The M2-PSMF filter is applied to acceleration signals. Acceleration error gain is selected as  $Q_i = 3.0$ . The mass of links 1 and 3 are modified to be  $m_1 = 2.3$  kg and  $m_3 = 2.75$  kg in the controller.

To further verify the repeatability of the above comparison, five tests are conducted for each method being used in obtaining results in Figures 9, 12 and 14 to provide a simple statistical overview of the performance. The absolute values of tracking errors (i.e.,  $\dot{x} - \dot{x}_c$ ) are shown in Figure 17. It is straightforward that the new sliding surface and variable sliding mode methods gain improved tracking accuracy. Moreover, the method that includes filtered acceleration feedback to equivalent control further enhances tracking accuracy and suppresses overshooting. It is important to note that outliers in the results of applying indirect tracking methods without AFC (i.e., methods in obtaining Figure 12) represent the overshooting signals. The average number of outliers for five tests of applying indirect tracking methods with AFC is less than 7%, which does not impact the interpretation of statistics.

In the end, the proposed control algorithm is employed to implement a human-following case to compare to simulation results in Figure 8b. During the interaction, the human participant randomly changed the grabbing force. Position tracking performance is as good as velocity tracking in the human-leading case, as shown in Figure 18. PER suppresses too fast increasing stiffness due to a higher time rate of change of interaction force.

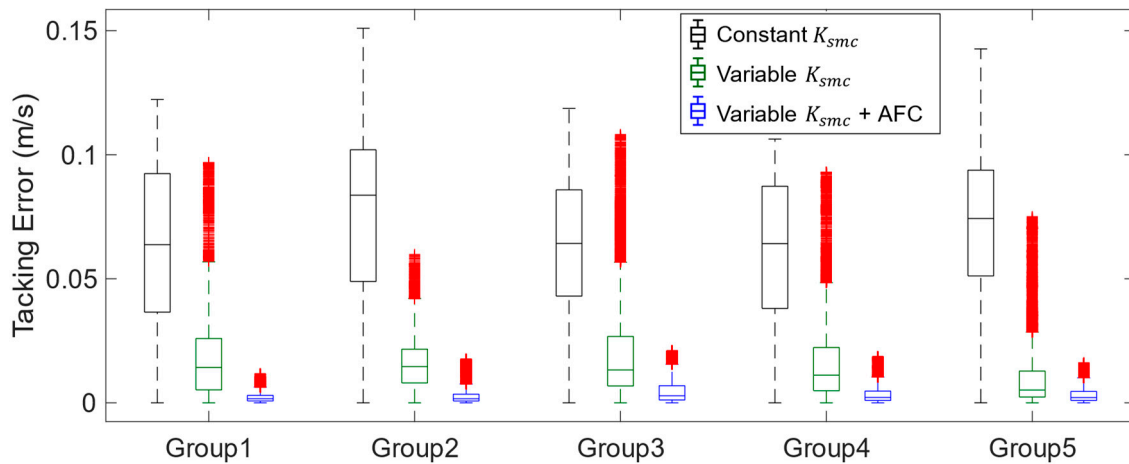


**Figure 17.** Statistical overview of repeatable experimental results of using indirect tracking approach with constant  $K_{smc}$ , variable  $K_{smc}$  without AFC, and variable  $K_{smc}$  with AFC methods. Each method corresponds to the method being employed to obtain results in Figures 9, 12 and 14, respectively.

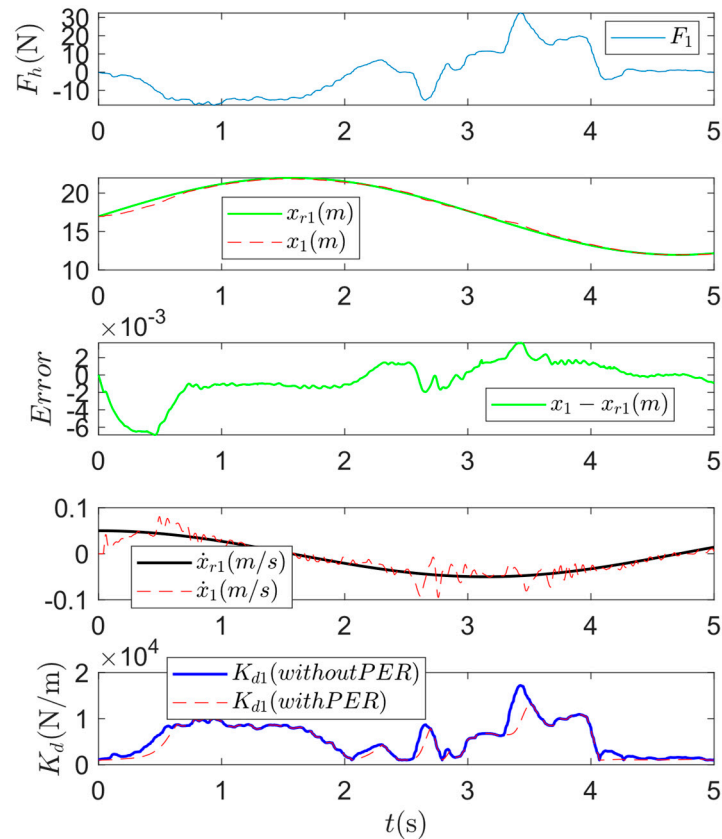


**Figure 18.** Tracking performance of indirect tracking approach with AFC for human-following VAC. The M2-PSMF filter is applied to acceleration signals. Acceleration error gain is selected as  $Q_i = 3.0$ . The mass of links 1 and 3 are modified to be  $m_1 = 2.3$  kg and  $m_3 = 0.65$  kg.

**5. Conclusions**

The work presented in this paper provides the theoretical proof and experimental validation of a new sliding mode control approach that addresses human intention adaptation, tracking accuracy, and system stability for variable admittance control in physical human–robot interaction. With the motivation of realizing stable user-desired responses of the robot during physical interaction via variable admittance control, a new sliding

surface is proposed. Its capability in realizing desired variable admittance response in both human-leading and human-following cases is theoretically proved regardless of the order of admittance equation. Then, we propose a corresponding control law that includes an adaptive sliding mode gain. This gain takes into account uncertainties arising from several sources: time-varying admittance parameters, the non-unique solutions associated with the Coriolis and centrifugal matrices in higher DoF systems, and the time lag introduced by the use of filters. The reachability condition in the Lyapunov sense is used to derive the variable sliding mode gain. A variable boundary layer method is then proposed to update boundary layer thickness according to the modeled time-varying uncertainties to address the issue of achieving a trade-off between chattering-free and accurate tracking. In the end, acceleration feedback is adopted in equivalent control to improve tracking performance further.

Through the comparative study, the improvement in tracking accuracy and chattering removal is apparently observed when the proposed approach is applied. Theoretical analysis, numerical simulation, and experimental results agree with one another, demonstrating our approach's effectiveness. In addition, a validation of acceleration feedback control in improving the control performance of SMC in VAC is also verified experimentally. To sum up, this study establishes a foundation for improving stability and robustness of variable admittance control using sliding mode. Real-world applications could be implemented by extending this fundamental study.

**Author Contributions:** Conceptualization, J.C. and P.I.R.; methodology, J.C. and P.I.R.; software, J.C.; validation, J.C. and P.I.R.; formal analysis, J.C. and P.I.R.; investigation, J.C. and P.I.R.; writing—original draft preparation, J.C.; writing—review and editing, P.I.R.; visualization, J.C.; supervision, P.I.R. All authors have read and agreed to the published version of the manuscript.

**Funding:** This research received no external funding.

**Institutional Review Board Statement:** Not applicable.

**Informed Consent Statement:** Informed consent was obtained from all subjects involved in the study.

**Data Availability Statement:** Data sharing is not applicable to this article.

**Acknowledgments:** The authors would like to acknowledge the financial support offered by Baylor University.

**Conflicts of Interest:** The authors declare no conflict of interest.

## Appendix A

### Proof of Universal Characteristic of the New Sliding Surface in Human-Following Case:

Consider the sliding surface for realizing desired admittance for human-leading case:

$$\sigma = M_d(t)(\dot{x} - \dot{x}_r) + D_d(t)(x - x_r) + \int K_d(t)(x - x_r)dt - \int f_h dt - (M_d(t)(\dot{x}_c - \dot{x}_r) + D_d(t)(x_c - x_r) + \int K_d(t)(x_c - x_r)dt - \int f_h dt) \quad (A1)$$

Applying integration by parts to Equation (A1) yields

$$\sigma = \int (M_d(t)(\ddot{x} - \ddot{x}_r) + D_d(t)(\dot{x} - \dot{x}_r) + K_d(t)(x - x_r))dt - \int (M_d(t)(\ddot{x}_c - \ddot{x}_r) + D_d(t)(\dot{x}_c - \dot{x}_r) + K_d(t)(x_c - x_r))dt \\ = \left[ M_d(t)(\dot{x} - \dot{x}_r) - \int \dot{M}_d(t)(\dot{x} - \dot{x}_r)dt + D_d(t)(x - x_r) - \int \dot{D}_d(t)(x - x_r)dt + \int K_d(t)(x - x_r)dt \right] \\ - \left[ M_d(t)(\dot{x}_c - \dot{x}_r) - \int \dot{M}_d(t)(\dot{x}_c - \dot{x}_r)dt + D_d(t)(x_c - x_r) - \int \dot{D}_d(t)(x_c - x_r)dt + \int K_d(t)(x_c - x_r)dt \right] \quad (A2)$$

Taking time derivative to Equation (A2) obtains

$$\begin{aligned} \dot{\sigma} &= \left[ \dot{M}_d(t)(\dot{x} - \dot{x}_r) - M_d(t)(\ddot{x} - \ddot{x}_r) - \dot{M}_d(t)(\dot{x} - \dot{x}_r) + \dot{D}_d(t)(x - x_r) - D_d(t)(\dot{x} - \dot{x}_r) - \dot{D}_d(t)(x - x_r) \right. \\ &\quad \left. + K_d(t)(x - x_r) \right] \\ &\quad - \left[ \dot{M}_d(t)(\dot{x}_c - \dot{x}_r) - M_d(t)(\ddot{x}_c - \ddot{x}_r) - \dot{M}_d(t)(\dot{x}_c - \dot{x}_r) + \dot{D}_d(t)(x_c - x_r) - D_d(t)(\dot{x}_c - \dot{x}_r) \right. \\ &\quad \left. - \dot{D}_d(t)(x_c - x_r) + K_d(t)(x_c - x_r) \right] \\ &= M_d(t)(\ddot{x}_c - \ddot{x}) + D_d(t)(\dot{x}_c - \dot{x}) + K_d(t)(x_c - x) \end{aligned} \tag{A3}$$

$\dot{\sigma} = 0$  gives the equivalent control

$$u_{eq} = H_w(x) \left( \ddot{x}_c + M_d^{-1}(t)D_d(t)\dot{x}_c - M_d^{-1}(t)D_d(t)\dot{x} + M_d^{-1}(t)K_d(t)x_c - M_d^{-1}(t)K_d(t)x \right) + C_w(x, \dot{x})\dot{x} + G_w(x) - f_h \tag{A4}$$

Substituting

$$\ddot{x}_c = \ddot{x}_r - M_d^{-1}(t)D_d(t)(\dot{x}_c - \dot{x}_r) - M_d^{-1}(t)K_d(t)(x_c - x_r) + M_d^{-1}(t)f_h \tag{A5}$$

into Equation (A5) yields

$$u_{eq} = H_w(x) \left( -M_d^{-1}(t)D_d(t)\dot{x} - M_d^{-1}(t)K_d(t)x + M_d^{-1}(t)f_h \right) + C_w(x, \dot{x})\dot{x} + G_w(x) - f_h \tag{A6}$$

Then, an equivalent acceleration term is defined according to feedback linearization as

$$\ddot{x}_s = \ddot{x}_r - M_d^{-1}(t)D_d(t)\dot{\tilde{x}} - M_d^{-1}(t)K_d(t)\tilde{x} + M_d^{-1}(t)f_h \tag{A7}$$

If  $\ddot{x}_s = \ddot{x}$ , Equation (A3) is equivalent to

$$\dot{\sigma} = M_d(t)(\ddot{x}_c - \ddot{x}_r) + D_d(t)(\dot{x}_c - \dot{x}_r) + K_d(t)(x_c - x_r) - f_h \tag{A8}$$

which is equal to zero. Hence, Equation (A3) is equal to zero if and only if  $x = x_c$ . Therefore, the sliding surface is defined as

$$\sigma = \dot{x} - \dot{x}_s \tag{A9}$$

which is the same as the one in the human-leading case. If system states stay on the sliding surface, both desired admittance and tracking of desired response can be realized.

## Appendix B

### Derivation of Variable Sliding Mode Gain with Acceleration Feedback:

Assuming the exact dynamics of the robot are known and no disturbances, the equivalent control is given as

$$u_{eq1} = H_w(x)\ddot{x} + S_w(x, \dot{x}) + G_w(x) - f_h \tag{A10}$$

Including acceleration feedback, Equation (A10) becomes

$$u_{eq2} = H_w \left( \ddot{x}_s - Q\ddot{\tilde{x}} \right) + C_w\dot{x}_s + G_w - f_h \tag{A11}$$

Rewrite Equation (A11) as

$$\ddot{x}_s = H_w^{-1}u_{eq2} - H_w^{-1}(S_w + G_w - f_h) + Q\ddot{\tilde{x}} \tag{A12}$$

Substituting  $-H_w^{-1}(S_w + G_w - f_h)$  solved from Equation (A10) into Equation (A12), the following expression is obtained:

$$(1 + Q)\dot{\sigma} = H_w^{-1}(u_{eq2} - u_{eq1}) \tag{A13}$$

Since  $\dot{\sigma} = 0$  is the prerequisite condition for obtaining equivalent control; it concludes that  $\mathbf{u}_{eq2} = \mathbf{u}_{eq1}$ . It is interesting to note that acceleration feedback only contributes to expanding system bandwidth rather than impacting system dynamics.

For stability of the new control law, one Lyapunov candidate function is selected as

$$V(\sigma) = \frac{1}{2} \sigma_{acc}^T \mathbf{H}_w \sigma \tag{A14}$$

where  $\sigma_{acc} = (\mathbf{I} + \mathbf{Q})\sigma$ . Taking the time derivative and applying the skew-symmetric property of  $\dot{\mathbf{H}}_w(\mathbf{x}) - 2\mathbf{C}_w^*(\mathbf{x}, \dot{\mathbf{x}})$  arrives at

$$\begin{aligned} \dot{V}(\sigma) &= \sigma_{acc}^T (\mathbf{H}_w \dot{\sigma} + \mathbf{C}_w^* \sigma) \\ &= \sigma_{acc}^T (\mathbf{H}_w \ddot{\mathbf{x}} - \mathbf{H}_w \ddot{\mathbf{x}}_s + \mathbf{C}_w^* \dot{\mathbf{x}} - \mathbf{C}_w^* \dot{\mathbf{x}}_s) \\ &= \sigma_{acc}^T (\mathbf{u} + \mathbf{f}_h - \mathbf{G}_w - \mathbf{H}_w \ddot{\mathbf{x}}_s - \mathbf{C}_w^* \dot{\mathbf{x}}_s) \end{aligned} \tag{A15}$$

Substituting

$$\mathbf{u} = \hat{\mathbf{H}}_w \ddot{\mathbf{x}}_s + \hat{\mathbf{S}}_w + \hat{\mathbf{G}}_w - \Delta - \mathbf{f}_h - \mathbf{K}_{smc} \text{sign}(\sigma) \tag{A16}$$

into Equation (A15) leads to

$$\dot{V}(\sigma) = \sigma_{acc}^T (\Delta \mathbf{H}_w \ddot{\mathbf{x}}_s + \Delta \mathbf{S}_w + \Delta \mathbf{G}_w + \Delta - \mathbf{H}_w \mathbf{Q}(\ddot{\mathbf{x}} - \ddot{\mathbf{x}}_s) - \mathbf{K}_{smc} \text{sign}(\sigma)) \tag{A17}$$

where  $\Delta$  represents uncertainties and disturbances. Assuming the following inequalities

$$\begin{aligned} \|\Delta \mathbf{H}_w(\mathbf{x})\| &= \|\hat{\mathbf{H}}_w(\mathbf{x}) - \mathbf{H}_w(\mathbf{x})\| \leq \delta_H, \\ \|\Delta \mathbf{S}_w(\mathbf{x}, \dot{\mathbf{x}})\| &= \|\hat{\mathbf{S}}_w(\mathbf{x}, \dot{\mathbf{x}}) - \mathbf{S}_w(\mathbf{x}, \dot{\mathbf{x}})\| \leq \delta_S, \\ \|\Delta \mathbf{G}_w(\mathbf{x})\| &= \|\hat{\mathbf{G}}_w(\mathbf{x}) - \mathbf{G}_w(\mathbf{x})\| \leq \delta_G \end{aligned} \tag{A18}$$

where the norm operator represents the Euclidean norm. Substituting Equation (A18) into Equation (A17) arrives at

$$\dot{V} \leq \|\sigma^T\| (\delta_H \|\ddot{\mathbf{x}}_s\| + \delta_C + \delta_G + \delta - K_{smc}) \tag{A19}$$

where  $-(\mathbf{H}_w \mathbf{Q}(\ddot{\mathbf{x}} - \ddot{\mathbf{x}}_s))$  is eliminated, such that Equation (A19) is more strict with the presence of acceleration feedback.

### Appendix C

This appendix lists some key assumptions made in this study.

#### Assumption A1. $\mathbf{x} = \mathbf{x}_c$

Admittance control imposes constraints on the reference trajectory and expected trajectory of the robot when interacting with humans. This expected trajectory acts as the control commands directed to the robot. The objective of the SMC is to ensure that the robot's actual response aligns with this expected or desired outcome. Based on this premise, assuming  $\mathbf{x} = \mathbf{x}_c$  basically sets a control goal. As a result, a specific sliding surface (i.e., Equation (15)) can be derived. This ensures two main objectives are met: (i) achieving the desired admittance; (ii) ensuring that the robot's response tracks the desired outcome under variable admittance control.

#### Assumption A2. $\mathbf{C}_w^*$ can be modeled as a source of bounded uncertainty

In many robotic systems, particularly higher DOF systems, the Coriolis and centrifugal term is not unique; that is, multiple matrices can satisfy the equations of motion. This is a result of the properties of the equations of motion and the flexibility in how they can be represented. The skew-symmetric property of  $(\dot{\mathbf{H}}_w - 2\mathbf{C}_w)$  is only valid for a unique  $\mathbf{C}_w$ . However, the analytical expression of unique  $\mathbf{C}_w$  (i.e.,  $\mathbf{C}_w^*$ ) is practically difficult to obtain. The Corio-

lis and centrifugal term ( $C(q, \dot{q})$ ) implicitly appears in the equivalent control in sliding mode control for manipulator in the Cartesian Space (e.g.,  $u_{eq} = H_w(x)\ddot{x} + S_w(x, \dot{x}) + G_w(x) - f_H$ ,  $S_w = -J^{-1T}H(q)J^{-1}JJ^{-1} + J^{-1T}C(q, \dot{q})J^{-1}$ , which contributes to deriving the sliding mode gain. In Equation (39),  $C_w^*$  is bounded as long as the entire system is stable. Moreover,  $\sigma$  is also bounded and approaches zero. Therefore, it is fair to assume that  $C_w^*\sigma$  is bounded, such that it can be modeled as bounded uncertainty.

**Assumption A3.**  $K_{smc}(x) = K_{smc}(x_s)$

In Equation (25),  $\ddot{x}_s$  is derived as the equivalent acceleration signal. Equation (25) represents perfect tracking of desired admittance response if  $\ddot{x}_s = \ddot{x}$ . A corresponding sliding surface is defined as Equation (26). Considering the finite reach time of sliding mode control and subtraction (i.e.,  $K_{smc}(x) - K_{smc}(x_s)$ ) in Equation (49), it can be fairly assumed that  $K_{smc}(x) = K_{smc}(x_s)$  during the sliding mode under constraints of the boundary layer. This assumption results in Equations (50) and (51), in which  $K_{smc}$  is a low-pass-filtered version of  $K_{smc}^0$ .  $K_{smc}^0$ , calculated from Equation (31), which is a conservative sliding mode gain, guarantees system stability. Hence, the new low-pass-filtered gain does not distort the stability condition. In addition, the boundary layer becomes a function of sliding mode gain, such that it takes system uncertainties into account and is adapted to system dynamic changes.

## References

1. Krüger, J.; Lien, T.K.; Verl, A. Cooperation of human and machines in assembly lines. *CIRP Ann.* **2009**, *58*, 628–646. [\[CrossRef\]](#)
2. Mörtl, A.; Lawitzky, M.; Kucukyilmaz, A.; Sezgin, M.; Basdogan, C.; Hirche, S. The role of roles: Physical cooperation between humans and robots. *Int. J. Robot. Res.* **2012**, *31*, 1656–1674. [\[CrossRef\]](#)
3. Solanes, J.E.; Gracia, L.; Munoz-Benavent, P.; Miro, J.V.; Carmichael, M.G.; Tornero, J. Human–robot collaboration for safe object transportation using force feedback. *Robot. Auton. Syst.* **2018**, *107*, 196–208. [\[CrossRef\]](#)
4. Xing, H.; Torabi, A.; Ding, L.; Gao, H.; Li, W.; Mushahwar, V.K.; Tavakoli, M. Human-robot collaboration for heavy object manipulation: Kinesthetic teaching of the role of wheeled mobile manipulator. In Proceedings of the 2021 IEEE/RSJ International Conference on Intelligent Robots and Systems (IROS), Prague, Czech Republic, 27 September–1 October 2021; pp. 2962–2969.
5. Xing, H.; Torabi, A.; Ding, L.; Gao, H.; Deng, Z.; Mushahwar, V.K.; Tavakoli, M. An admittance-controlled wheeled mobile manipulator for mobility assistance: Human–robot interaction estimation and redundancy resolution for enhanced force exertion ability. *Mechatronics* **2021**, *74*, 102497. [\[CrossRef\]](#)
6. Xing, H.; Ding, L.; Gao, H.; Li, W.; Tavakoli, M. Dual-user haptic teleoperation of complementary motions of a redundant wheeled mobile manipulator considering task priority. *IEEE Trans. Syst. Man Cybern. Syst.* **2022**, *52*, 6283–6295. [\[CrossRef\]](#)
7. Liu, Z.; Hao, J. Intention recognition in physical human-robot interaction based on radial basis function neural network. *J. Robot.* **2019**, *2019*, 4141269. [\[CrossRef\]](#)
8. Park, J.S.; Park, C.; Manocha, D. I-planner: Intention-aware motion planning using learning-based human motion prediction. *Int. J. Robot. Res.* **2019**, *38*, 23–39. [\[CrossRef\]](#)
9. Tortora, S.; Michieletto, S.; Stival, F.; Menegatti, E. Fast human motion prediction for human-robot collaboration with wearable interface. In Proceedings of the 2019 IEEE International Conference on Cybernetics and Intelligent Systems (CIS) and IEEE Conference on Robotics, Automation and Mechatronics (RAM), Bangkok, Thailand, 18–20 November 2019; pp. 457–462.
10. Li, S.; Zhang, L.; Diao, X. Deep-learning-based human intention prediction using RGB images and optical flow. *J. Intell. Robot. Syst.* **2020**, *97*, 95–107. [\[CrossRef\]](#)
11. Krishnan, R.H.; Pugazhenthii, S. Mobility assistive devices and self-transfer robotic systems for elderly, a review. *Intell. Serv. Robot.* **2014**, *7*, 37–49. [\[CrossRef\]](#)
12. Yan, T.; Cempini, M.; Oddo, C.M.; Vitiello, N. Review of assistive strategies in powered lower-limb orthoses and exoskeletons. *Robot. Auton. Syst.* **2015**, *64*, 120–136. [\[CrossRef\]](#)
13. Windrich, M.; Grimmer, M.; Christ, O.; Rinderknecht, S.; Beckerle, P. Active lower limb prosthetics: A systematic review of design issues and solutions. *Biomed. Eng. Online* **2016**, *15*, 5–19. [\[CrossRef\]](#)
14. Han, J.H.; Lee, S.J.; Kim, J.H. Behavior hierarchy-based affordance map for recognition of human intention and its application to human–robot interaction. *IEEE Trans. Hum.-Mach. Syst.* **2016**, *46*, 708–722. [\[CrossRef\]](#)
15. Chen, J.; Ro, P.I. A Conceptual Approach of Passive Human-Intention-Orientated Variable Admittance Control using Power Envelope. In Proceedings of the 2021 IEEE/RSJ International Conference on Intelligent Robots and Systems (IROS), Prague, Czech Republic, 27 September–1 October 2021; pp. 7300–7306.
16. Chen, J.; Ro, P.I. Human intention-oriented variable admittance control with power envelope regulation in physical human-robot interaction. *Mechatronics* **2022**, *84*, 102802. [\[CrossRef\]](#)

17. Müller, F.; Janetzky, J.; Behrnd, U.; Jäkel, J.; Thomas, U. User force-dependent variable impedance control in human-robot interaction. In Proceedings of the 2018 IEEE 14th International Conference on Automation Science and Engineering (CASE), Munich, Germany, 20–24 August 2018; pp. 1328–1335.
18. Cacace, J.; Finzi, A.; Lippiello, V. Enhancing shared control via contact force classification in human-robot cooperative task execution. In *Human Friendly Robotics*; Springer: Cham, Switzerland, 2019; pp. 167–179.
19. Hogan, N. Impedance control: An approach to manipulation. In Proceedings of the 1984 American Control Conference, San Diego, CA, USA, 6–8 June 1984; pp. 304–313.
20. Ott, C.; Mukherjee, R.; Nakamura, Y. Unified impedance and admittance control. In Proceedings of the 2010 IEEE International Conference on Robotics and Automation, Anchorage, AK, USA, 3–7 May 2010; pp. 554–561.
21. Keemink, A.Q.; van der Kooij, H.; Stienen, A.H. Admittance control for physical human–robot interaction. *Int. J. Robot. Res.* **2018**, *37*, 1421–1444. [[CrossRef](#)]
22. Duchaine, V.; Gosselin, C. Safe, stable and intuitive control for physical human-robot interaction. In Proceedings of the 2009 IEEE International Conference on Robotics and Automation, Kobe, Japan, 12–17 May 2009; pp. 3383–3388.
23. Li, Z.; Huang, B.; Ye, Z.; Deng, M.; Yang, C. Physical human–robot interaction of a robotic exoskeleton by admittance control. *IEEE Trans. Ind. Electron.* **2018**, *65*, 9614–9624. [[CrossRef](#)]
24. Li, K.; Chen, R.; Nuchkrua, T.; Boonto, S. Dual loop compliant control based on human prediction for physical human-robot interaction. In Proceedings of the 2019 58th Annual Conference of the Society of Instrument and Control Engineers of Japan (SICE), Hiroshima, Japan, 10–13 September 2019; pp. 459–464.
25. Lecours, A.; Mayer-St-Onge, B.; Gosselin, C. Variable admittance control of a four-degree-of-freedom intelligent assist device. In Proceedings of the 2012 IEEE International Conference on Robotics and Automation, Saint Paul, MN, USA, 14–18 May 2012; pp. 3903–3908.
26. Sharkawy, A.N.; Koustoumpardis, P.N.; Aspragathos, N. A neural network-based approach for variable admittance control in human–robot cooperation: Online adjustment of the virtual inertia. *Intell. Serv. Robot.* **2020**, *13*, 495–519. [[CrossRef](#)]
27. Li, Y.; Ge, S.S. Human-Robot Collaboration Based on Motion Intention Estimation. *IEEE/ASME Trans. Mechatron.* **2013**, *19*, 1007–1014. [[CrossRef](#)]
28. Itadera, S.; Kobayashi, T.; Nakanishi, J.; Aoyama, T.; Hasegawa, Y. Impedance control based assistive mobility aid through online classification of user’s state. In Proceedings of the 2019 IEEE/SICE International Symposium on System Integration (SII), Paris, France, 14–16 January 2019; pp. 243–248.
29. Dimeas, F.; Aspragathos, N. Online stability in human-robot cooperation with admittance control. *IEEE Trans. Haptics* **2016**, *9*, 267–278. [[CrossRef](#)]
30. Kronander, K.; Billard, A. Stability considerations for variable impedance control. *IEEE Trans. Robot.* **2016**, *32*, 1298–1305. [[CrossRef](#)]
31. Ferraguti, F.; Talignani Landi, C.; Sabattini, L.; Bonfè, M.; Fantuzzi, C.; Secchi, C. A variable admittance control strategy for stable physical human–robot interaction. *Int. J. Robot. Res.* **2019**, *38*, 747–765. [[CrossRef](#)]
32. Park, J.; Choi, Y. Input-to-state stability of variable impedance control for robotic manipulator. *Appl. Sci.* **2020**, *10*, 1271. [[CrossRef](#)]
33. Slotine, J.J.E.; Li, W. *Applied Nonlinear Control*; Prentice Hall: Englewood Cliffs, NJ, USA, 1991; Volume 199, p. 705.
34. Bucak, İ.Ö. An In-Depth Analysis of Sliding Mode Control and Its Application to Robotics. In *Automation and Control*; IntechOpen: London, UK, 2020.
35. Lu, Z.; Goldenberg, A.A. Robust impedance control and force regulation: Theory and experiments. *Int. J. Robot. Res.* **1995**, *14*, 225–254.
36. Tu, Y.; Zhu, A.; Song, J.; Shen, H.; Shen, Z.; Zhang, X.; Cao, G. An adaptive sliding mode variable admittance control method for lower limb rehabilitation exoskeleton robot. *Appl. Sci.* **2020**, *10*, 2536. [[CrossRef](#)]
37. Torabi, M.; Sharifi, M.; Vossoughi, G. Robust adaptive sliding mode admittance control of exoskeleton rehabilitation robots. *Sci. Iran.* **2018**, *25*, 2628–2642. [[CrossRef](#)]
38. Liu, J.; Wang, X. *Advanced Sliding Mode Control for Mechanical Systems*; Springer: Berlin, Germany, 2012; pp. 31–35.
39. Fazli, E.; Rakhtala, S.M.; Mirrashid, N.; Karimi, H.R. Real-time implementation of a super twisting control algorithm for an upper limb wearable robot. *Mechatronics* **2022**, *84*, 102808. [[CrossRef](#)]
40. Han, J.D.; Wang, Y.C.; Tan, D.L.; Xu, W.L. Acceleration feedback control for direct-drive motor system. In Proceedings of the 2000 IEEE/RSJ International Conference on Intelligent Robots and Systems (IROS 2000) (Cat. No. 00CH37113), Takamatsu, Japan, 31 October–5 November 2000; Volume 2, pp. 1068–1074.
41. Sedghi, B.; Bauvir, B.; Dimmler, M. Acceleration feedback control on an AT. In *Ground-Based and Airborne Telescopes II*; SPIE: Bellingham, WA, USA, 2008; Volume 7012, pp. 704–715.
42. Ma, J.; Yao, Y.; Liu, K. Sliding mode control with angular acceleration feedback for a flight motion simulator. In Proceedings of the 2009 41st Southeastern Symposium on System Theory, Tullahoma, TN, USA, 15–17 March 2009; pp. 190–194.
43. Aung, M.T.S.; Shi, Z.; Kikuuwe, R. A new parabolic sliding mode filter augmented by a linear low-pass filter and its application to position control. *J. Dyn. Syst. Meas. Control.* **2018**, *140*, 041005. [[CrossRef](#)]
44. Studenny, J.; Belanger, P.R. Robot manipulator control by acceleration feedback: Stability, design and performance issues. In Proceedings of the 1986 25th IEEE Conference on Decision and Control, Athens, Greece, 10–12 December 1986; pp. 80–85.

45. Buss, S.R. Introduction to inverse kinematics with jacobian transpose, pseudoinverse and damped least squares methods. *IEEE J. Robot. Autom.* **2004**, *17*, 16.
46. Xing, H.; Torabi, A.; Ding, L.; Gao, H.; Li, W.; Tavakoli, M. Enhancing kinematic accuracy of redundant wheeled mobile manipulators via adaptive motion planning. *Mechatronics* **2021**, *79*, 102639. [[CrossRef](#)]

**Disclaimer/Publisher's Note:** The statements, opinions and data contained in all publications are solely those of the individual author(s) and contributor(s) and not of MDPI and/or the editor(s). MDPI and/or the editor(s) disclaim responsibility for any injury to people or property resulting from any ideas, methods, instructions or products referred to in the content.